Statistical Mechanics of Mixtures of Many Components

Master thesis in physics

submitted to Fachbereich Physik, Mathematik und Informatik (FB 08)
Johannes-Gutenberg Universität Mainz

by

Felix Herrmann

March 2nd, 2023

supervised by

Prof. Dr. Burkhard Dünweg
Prof. Dr. Friederike Schmid

Joint collaboration of the MPI-P and JGU Mainz

Ich versichere, dass ich die Arbeit selbstständig verfasst und keine anderen als die angegebenen Quellen und Hilfsmittel benutzt sowie Zitate kenntlich gemacht habe.

Mainz, den 02.05.2023

Felix Herrmann
KOMET
Institut für Physik
Staudingerweg 7
Johannes Gutenberg-Universität D-55099 Mainz
feherrma@students.uni-mainz.de

Contents

Abstract

Phase behavior observed in biology remains puzzling. For instance, the plasma membrane of cells exhibits signs of criticality, as it is controlled to remain near a demixing point. This membrane contains thousand of components, and it is largely unclear how its composition is controlled. Beyond this, one can ask whether cells should obey the traditional thermodynamic picture, given their small size, large number of components and the presence of non-equilibrium processes.

Here, we study toy systems, lattice models containing many (>30) components. We show that these systems exhibit strong finite-size effects. These manifest as behavior that appears similar to traditional critical behavior, but vanish logarithmically with system size. We examine scaling laws, and whether traditional paradigms from macroscopic thermodynamics can be broken in such systems.

1 Introduction

The cell is the basic unit of life. In eukaryotes its fluid membrane separates the cytoplasm from the environment and forms a complex interface with functions such as filtration and communication. It is embedded in a constantly changing environment and consists of a vast variety of different molecules. Additionally its components get constantly removed, added or exchanged [1] which adds further complexity. The understanding of a membrane of many constituents with complex interactions is important because the cells health depends on its membrane functioning normally. Nonetheless the behaviour of such complex membranes is still largely unexplored.

It has been hypothesized that cell membranes posses some lateral homogeneity through different liquid phases [2]. Functional platforms termed 'lipid rafts' could persist to facilitate reactions with molecules in the environment as well as exo- and endocytosis. These represent liquid ordered phases in a liquid disordered environment. One of the possible explanations is that the cell membrane is near a critical point in composition under physiological conditions [3]. Proximity to a critical point would imply enhanced correlation lengths and fluctuations on larger scales which has many advantages for membrane organization in cells. But keeping the membrane close to criticality seems like a difficult task as the many membrane components have to be tuned just to the right composition under constantly changing external conditions.

In the past the phase behaviour of these complex membranes has usually been studied by simplification to ternary mixtures since each new components adds a further dimension to the problem. These models consist of a component with high melting temperature T_m, a component with low T_m and cholesterol. They display critical demixing with a critical point depending on their composition [4]. While they capture the basic phase behaviour of cell membranes the resulting phases are more structured than what is observed in recent experiments. In real cell membranes the phases display nematic disorder below the critical temperature indicating a over-simplification by ternary mixtures [5].

Some time ago an experimental technique to study cell membranes with adequate composition has been developed [6]. Giant plasma membrane vesicles (GPMVs) are extracted from living cells such that their composition represents that of living cells. When these vesicles get cooled 10-15K below growth temperature they display a demixing transition with typical 2D Ising critical exponents, thus supporting the critical hypothesis [7] [8]. Cells seem to be able to adapt their membrane composition depending on the environment such that they remain critical, making use of many different components which seem to relax the need for precise component control. This further questions the validity of ternary mixtures as model membranes as they need to be precisely tuned in composition.

This project continues a previous study in which the phase behaviour of such membranes was investigated by a 2D lattice model which focuses on the effect of the large variety of membrane constituents [9]. Lattice models are powerful tools to study phase behaviour since they drastically reduce the degrees of freedom of

a system while making it possible to do finite size scaling up to large systems. Many real systems can be mapped onto such lattices by only regarding the important features for their collective behaviour. This drastically reduces the computational costs. Since a demixing transition is expected the model is a generalization of the 2D Ising model to N available spin states. It can be mapped onto a membrane with a fixed number of N chemically different lipids which can be transformed into one another by some chemical reaction which is controlled by a chemical potential for each lipid. The spin values can be mapped e.g. onto the degree of lipid saturation where it is energetically favourable for lipids with similar saturation to group. This system displays distinct features in the *continuous* limit $N \longrightarrow \infty$ as to the case where N is small (e.g. $N = 2$). Below a system-size depending onset temperature T_{fs} the *continuous* system displays finite size effects, such as system spanning correlations over a temperature range and non-ergodicty, which vanish in the thermodynamic limit. Instead of an ordered phase we observe a quasi-ordered phase with orientational disorder.

The model reproduces many of the trends found in GPMV experiments such as a growth-temperature depended demixing temperature and composition regulation near criticality. A critical exponent was found for the demixing transition which deviates from the 2D Ising universality class but further apparent scaling laws below T_{fs} were observed which could be responsible for the deviation by finite size effects. Additionally the behaviour was found to be qualitatively invariant under exact form of the hamiltonian of the model as long as it is translational invariant making it robust to the exact values of chemical potentials for each lipid as well as for their interactions.

In the first part of this work we try to generalize this model to a 2D order parameter which could be used to add e.g. charged head-group interactions to the model. For this purpose we use the 2D XY model. We observe the same quantitative behaviour for both models indicating an independence of the behaviour of order parameter dimension. The same critical exponent for one of the apparent scaling laws was found suggesting *'broken'* universality below T_{fs}. Secondly, we try to find the origin of that apparent scaling law by characterizing the instantaneous spin distributions. Their moments indicate Gaussian-like behaviour and we employ an analytically solvable model for this purpose; a Gaussian-like model. One of the apparent scaling laws turns out to be a finite size effect of logarithmic origin in this model but independence of spin order dimension becomes trivial. It is unclear however if this model fully covers all aspects of the previously induced model as it is free of cross-correlations.

Cells are small objects and fall into the peculiar finite size regime introduced above and we are curious which finite size effects they can use to organise their membrane and what the experimental signatures would be.

2 Statistical Mechanics

In order to understand the physical approaches and reasoning used in this study we first lay out the relation between thermodynamics and statistical mechanics. Then we introduce the notion of lattice models in statistical mechanics and how they can be mapped onto statistical ensembles. By doing so we get to know some of the important techniques to study such systems and remember some important insights into the field like finite size scaling and universality. Finally we introduce the lattice models subject in this thesis - continuous spin models.

2.1 Thermodynamics and Statistical Mechanics

In thermodynamics a system like a box of gas particles is described by a few *macroscopic* variables such as the internal energy E, the volume V, temperature T, number of particles N and so on. In classical statistical mechanics the macroscopic behaviour of a system is derived from the motion of its many components e.g. molecules in a glass of water. To obtain a good approximation of thermodynamic observables of such systems we are interested in the thermodynamic limit where $N \longrightarrow \infty$, $V \longrightarrow \infty$ such that $N/V =$ constant [10]. Probabilistic arguments derived from stochastic considerations become effective tools as the standard deviation of a stochastic variable decays with the number of components:

$$\sigma = \sqrt{\frac{1}{N}\sum_{i=1}^{N}(x_i - \mu)^2}$$

where $\mu = \frac{1}{N}\sum_{i=1}^{N} x_i$ is the mean value for an observable measured N times. By the *law of large numbers* stochastic observables will converge towards a mean value if we repeat the same experiment many times [11]. But we are not able anymore to calculate exact quantities. But the *central limit theorem* ensures that our values for observables converge towards a normal distribution from which we can extract their mean and variance [12]. In thermal equilibrium the mean values will converge to a static value around which they fluctuate over time as the components of a system for any temperature $T > 0$ are in motion.

If we observe a thermodynamic system we will find it with some probability in a certain configuration or state, called *microstate*. We then take snapshots of its microstates over time, calculate the macroscopic quantities from the particles of a snapshot and average over all of the snapshots. But we can also imagine an infinite number of copies of the system each in a different microstate, present all at the same time. The microstates are possible configurations of the system compatible with the specific external conditions which affect the system and define a macrostate (see figure 1). Depending on the external parameters which affect the system we can define different *statistical ensembles*. For a given macrostate they make it possible to assign probabilities to all compatible microstates which makes it possible to extract thermodynamic quantities of the system which the statistical ensemble represents [13]. Statistical ensembles describe equilibrium phenomena.

Three main statistical ensembles are studied which are defined by different *thermodynamic potentials* and represent constrained systems. The internal energy U describes the effect of all possible *thermodynamic processes* which can affect a system (first thermodynamic law):

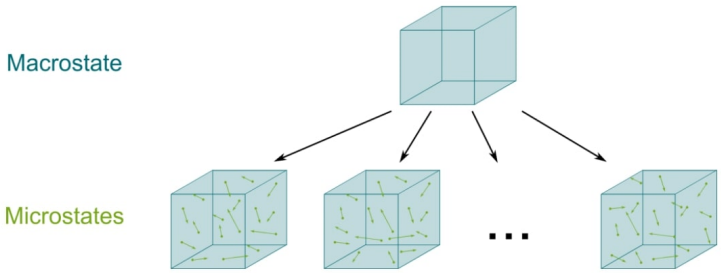

Figure 1: Macro- and microstates of a thermodynamic ensemble. The graphic depicts the consideration of all microstates at the same time compatible with the macrostate. Figure adapted from [14].

$$dU = \delta Q - \delta W + \sum_i \mu_i dN_i \tag{1}$$

Here δQ describes the infinitesimal heat transfer through configurational or temperature changes, δW the infinitesimal mechanical work done on the system through changes in volume or pressure and dN the exchange of particles e.g. through chemical reactions. δ is used to denote the path dependence of heat and work changes and describes an *inexact differential*. μ is called the chemical potential and quantifies the cost of adding or removing a particle from the system (or transformation into another particle type). When there is more than one particle type a sum is needed to account for particles with different chemical potentials which are related to each other (see Gibbs-Duhem relation [15]). The contributions to dU are pairs of *conjugate variables* similar to the formalism in mechanics: they are combinations of an intensive variable (non-additive thermodynamic 'forces' like temperature, pressure and chemical potential) and an extensive variable (additive like entropy, volume and particle number) leading to an extensive internal energy [13]. Similarly to mechanics a change in energy is the product of a force and a displacement.

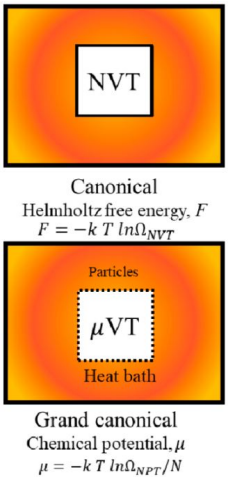

Figure 2: Example of two thermodynamic ensembles with their respective characteristic thermodynamic potential. The orange box depicts inexhaustible *baths*. Figure adapted from [16]

The **microcanonical** ensemble deals with isolated (non-interacting) systems. Its macrostate is defined by the total number of particles, the confining volume and the internal energy (N,V,E) which are fixed. Its appropriate thermodynamic potential (which describes changes in its energy) is the entropy S. The 2nd law of thermodynamics states that $dS \geq 0$ which describes the intuition that it is most probable to find repelling particles in the box evenly

distributed for any $T > 0$ [17]. For a microcanonical ensemble only changes in configuration are possible and thus a system will relax to its equilibrium by internal energy changes due to configurational changes only:

$$dU = TdS \tag{2}$$

The second model is the **canonical** ensemble where the particles can interchange energy with an ideal (inexhaustible) heat bath (see figure 2). It is characterised by the external variables (N,V,T) and its thermodynamic potential is given by the free energy:

$$F = U - TS$$

The system strives towards equilibrium with an external heat bath thus changing its internal energy by giving its components more mean kinetic energy which makes different microstates accessible. It is useful when describing a system where the temperature is changed.

The last ensemble I want to mention is the **grand-canonical** ensemble where the system can also interchange particles with an infinite reservoir and is described by (μ, V, T) and the *grand potential*:

$$\Phi_G = U - TS - \sum_i \mu_i N_i$$

In principle there are many more ensembles one can construct to efficiently extract the thermodynamic observables of interest depending on the external conditions. A nice thing about these ensembles is that we do not have to model the baths explicitly in practice but its enough to impose constrains with different thermodynamic potentials to efficiently obtain the correct observable values in the thermodynamic limit.

The relation of these ensembles to thermodynamic systems was first noted by L. Boltzmann and J.W. Gibbs [15] [54]. Boltzmann related the configurational entropy of a system to what he called the *multiplicity* Ω, which counts the number of available microstates for a given macrostate stochastically. For this, one has to partition the box which contains indistinguishable particles (see Gibbs paradox [19]) into small volumes of particle size which can either be occupied or unoccupied. It is given by:

$$S = k_B \log \Omega$$

Gas particles with a non-zero internal energy will spread out evenly in the volume as the number of possible configurations is higher. Since $dS > 0$ the system's entropy is maximal in thermal equilibrium. Gibbs noted that this entropy

is the thermodynamic potential for the microcanonical ensemble as its energy can only change through heat changes when T is constant (see eq. (2)). Thus establishing a connection between thermodynamics and statistical mechanics.

A useful quantity which fully describes an ensemble is the partition function [10]. It is the normalization factor in the probability of finding the system in a certain microstates among all other microstates compatible with a given macrostate. For a canonical ensemble it is given by

$$Z = \sum_i e^{-\beta F}$$

where $e^{-\beta F}$ is the Boltzmann distribution with inverse temperature $\beta = 1/(k_B T)$ and F is the appropriate thermodynamic potential; the Helmholtz free energy. The sum runs over all microstates of the ensemble. It can be derived by maximizing the entropy of two systems in thermal contact [10]. k_B is called the Boltzmann factor. The probability of finding a microstate is then given by

$$p_i = \frac{1}{Z} e^{-E_i/(k_B T)}$$

where E_i is the energy of microstate i. In this way we can assign probabilities to microstates under given external conditions and can see how p_i changes upon changing the external parameters.

The partition function takes different thermodynamic potentials in consideration depending on the statistical ensemble. While all the above ensembles seem to be very different they are all equivalent in the thermodynamic limit. Mathematically the ensembles are connected by Legendre transformations which induce different constrains [20]. Formally a Legendre transform transforms a variable of a convex function into its conjugate quantity. For example the fundamental equation for the internal energy is:

$$dU = TdS - PdV + \sum_i \mu_i dN_i$$

It is described by a set of natural variables (S, V, N_i) (extensive). By introducing additional pairs of conjugate variables we can define a new thermodynamic potential, for example the Helmholtz free energy:

$$F = U - TS$$

In differential form this can be written as

$$dF = -SdT - PdV + \sum_i \mu_i dN_i$$

which is now described by natural variables (T, V, N_i). Similarly one can derive the *Gibbs free energy*:

$$G(T, P, N_i) = F(T, V, N_i) + PV$$

$$\longrightarrow dG = -SdT + VdP + \sum_i \mu dN_i$$

Different thermodynamic potentials are suited well for extracting certain observables. For example a change in the Helmholtz free energy dF is related to a change in temperature or a change in volume (if we neglect chemical reactions). When fixing the temperature in the experiment we directly obtain the mechanical work $\delta W = -PdV$ done by the system by observing dF. Since the ensembles are all equivalent just the exact definitions of the observables change and we can choose a convenient thermodynamic potential.

Now coming back to the partition function; if Z is known then one can derive all thermodynamic quantities of the system in equilibrium as thermal averages and derivatives of Z as it is an equation of state. For example the total mean energy of the system can be calculate as:

$$\langle E \rangle = -\frac{\partial}{\partial \beta} \log Z$$

The brackets denote a *thermal average* over space and time. For a system in equilibrium fluctuations around this mean value can be seen as the response of the system to perturbations. These perturbations on the other hand can be caused by spontaneous fluctuations in the system itself which in turn perturb the system again through dissipation (e.g. friction). This is stated by the *fluctuation-dissipation theorem* [21] which relates *response functions* to fluctuations.

For energy fluctuations for example the response function is the heat capacity C (here at constant volume):

$$C_V = \frac{1}{k_B T} \frac{\partial^2 \log Z}{\partial \beta^2} = \left\langle (E - \langle E \rangle)^2 \right\rangle$$

For us they are important here since they give insight into the *critical behaviour* of a system as we will see later. The above relations imply that derivatives of Z with respect to some control parameter (here the inverse temperature) can be used to obtain statistical moments which describe observables and their fluctuations. It again highlights the connection between statistical mechanics and thermodynamics since the partition function is derived through stochastic considerations.

2.2 Phase Transitions

An interesting behaviour of thermodynamic systems is their ability to undergo *phase transitions* [22]. As the thermodynamic variables are changed the system changes its macroscopic behaviour.

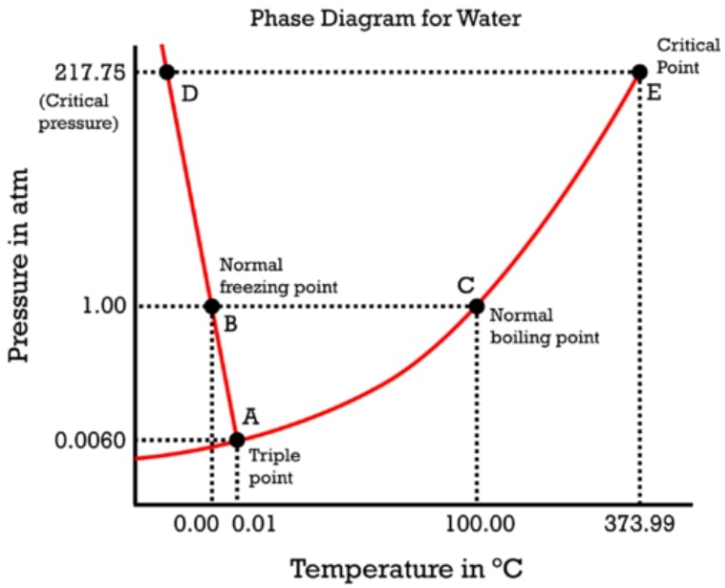

Figure 3: Phase diagram of water for intrinsic variables T and P. Figure adapted from [23].

Phases can be quantified by looking at an *order parameter* which takes on different values in different phases (see figure 5). As a typical example we will consider water where the density ρ can be used as an order parameter as its states (gas-, liquid- or solid-like) have very different densities. Its thermodynamic behaviour can be illustrated in a *phase diagram* of two intrinsic (non-additive) variables T and P (see figure 3).

At a phase transition the free energy of the system is not analytical as quantities which are derivatives of the free energy display a discontinuity. Two common types of phase transitions are 1st order (discontinuous) and 2nd order (continuous) transitions.

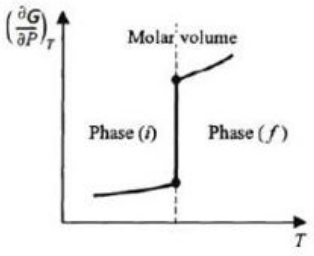

Figure 4: The molar volume can be obtained by differentiating the Gibbs free energy with respect to P at constant T. In a (V, T) diagram V displays a finite jump at the transition. Figure adapted from [25]

A first order transition can be characterized by a discontinuity in the first derivative in the thermodynamic potential which translates to a discontinuity in the corresponding state variable [24]. Examples are the melting or evaporation transition,

where the temperature stays constant but the volume changes abruptly (see figure 4). In figure 3 these correspond to the red lines.

A second order phase transition can be characterised by a discontinuity in the 2nd derivative of the free energy but the 1st derivative stays continuous. There exist points of intrinsic variables (e.g. (T_c, P_c)) where the free energy difference between different phases becomes negligible. These are called *critical points* and distinguishing different phases of a system becomes impossible. In figure 3 these are points where the coexistence lines end.

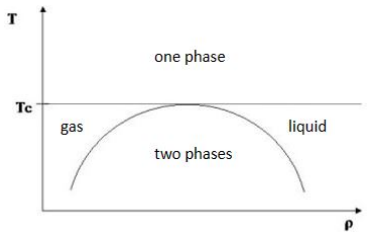

Figure 5: In this (ρ, T) plot a 2nd order phase transition occurs at T_c if the density is just right. Otherwise one goes to the two phase region by a first order phase transition, indicated by a coexistence parabola. Figure adapted from [26]

This phenomenon is accompanied by *critical opalescence*: water looks beclouded as correlations between the particles become system spanning and fluctuations on all scales are observed. This translates to diverging susceptibilities, compressibilities and heat capacities since they are related to fluctuations (2nd moments) in e.g. particle density or velocity.

As we will see later knowledge about the behaviour at the phase transition can be used to group different systems into broader 'simplified' groups of systems.

Also note that the true phase behaviour of a system can only exist in the thermodynamic limit as otherwise the finite size of the system can alter its behaviour through the boundaries. A boundary creates an interface which contributes to changes in the free energy $dF \propto \gamma dA$ where γ is the surface tension and dA is the increment in surface area. Picture for example a cubic lattice. As $V \longrightarrow \infty$ the contribution of this term vanishes as dA becomes more and more negligible compared to the overall volume since the boundaries only increase as $4L^2$ whereas the volume increases as L^3, where L is the length of the box. Also fluctuations can create interfaces but by a similar argument the central limit theorem predicts that their contribution vanishes in the thermodynamic limit as $\propto 1/\sqrt{N}$ where N is the number of components [10].

2.3 Lattice gas mapping

As we have seen, simulating phase transitions requires macroscopic systems. Thus it can become computational expensive to simulate phase transitions by the use of atomistic simulations. It is necessary to reduce the degrees of freedom for such systems to efficiently extract statistics. Therefor we want to reduce a system to its most important aspects which still capture the macroscopic behaviour correctly. For simulating phase transitions lattice systems become powerful tools. Here we will show that they can be mapped onto the thermodynamic ensembles introduced before.

Consider a single species of N gas particles in a box of size L with constraint $N =$ constant. For illustration we consider a $2d$ gas. We discretise the area in volumes of particle size and end up with a *lattice gas* (see figure 6). After discretization let $n_i = \{0, 1\}$ denote the occupation of a site ($n_i = 0$ unoccupied, $n_i = 1$ occupied). The energy of a gas of identical particles can be described by

$$E(\vec{r}_i) = \sum_{i<j} u(|\vec{r}_i - \vec{r}_j|)$$

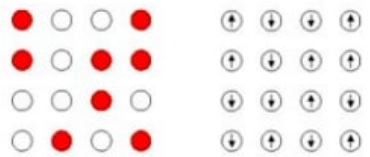

Figure 6: Sketch of a lattice gas (left) and spin lattice model (right). Figure adapted from [26]

where u is a potential which shall represent their interactions. For an ideal gas one can approximate this potential by a Lennard-Jones (LJ) potential (see figure 7). For a lattice gas we further approximate such a potential by letting only nearest neighbours interact (unoccupied sites do not interact (thus $n_i = 0$)). For $|\vec{r}_i - \vec{r}_j| < a$ we have to set $u \longrightarrow \infty$, where a is the lattice spacing. Translating the original potential to the lattice gas can be done by:

$$u(|\vec{r}_i - \vec{r}_j|) \longrightarrow u'(i,j) = \begin{cases} -\epsilon, & \text{if } (i,j) \text{ are nearest neighbors} \\ 0, & \text{otherwise} \end{cases}$$

where ϵ is the interaction strength between two particles.

Since the energy of the system only depends on the interactions of the particles we can think of a lattice gas Hamiltonian of the form:

$$\mathcal{H}_{gas} = -\epsilon \sum_{\langle i,j \rangle} n_i n_j$$

The sum runs over nearest neighbours $\langle i, j \rangle$. Again we have to consider all possible configurations of an ensemble with fixed number

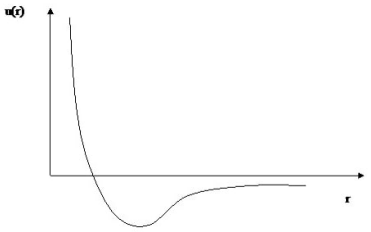

Figure 7: Form of the Lennard-Jones potential e.g. given by $V_{LJ}(r) = 4\epsilon\left[(\frac{\sigma}{r})^{12} - (\frac{\sigma}{r})^{6}\right]$, where ϵ is an interaction strength between the particles. Figure adapted from [26].

of particles to obtain the canonical partition function:

$$Z_C = \sum_{\sum_i n_i = N} e^{-\beta \mathcal{H}_{gas}}$$

where the sum is constrained to microstates with total particle number N.

We can now describe a lattice gas with identical particles in the grand canonical ensemble where the total number of particles is not fixed. We saw that we can do this by imposing different constrains on the ensemble and the grand canonical partition function is given by:

$$Z_{GC} = \sum_{n=0}^{N} z^N Z_C = \sum_{all\ config.} e^{-(\beta H_{gas} - \mu \sum_i n_i)}$$

where N is the total number of particles in the system. The sum is now unconstrained and runs over all possible configurations. μ is again the chemical potential which depends on temperature and the concentration of the particles but is equivalent for all particles of the same type. $z = e^{\beta\mu}$ is called the fugacity and connects the canonical ensemble with the grand-canonical ensemble. Note that the fugacity can be rewritten as $k_B T \log(z) = \mu$. We can now introduce an effective Hamiltonian $\mathcal{H}_{eff} = \mathcal{H}_{gas} - \mu \sum_i n_i$.

Now we can make the transition to a spin lattice. Here we identify an occupied site by $s_i = +1$ and an unoccupied site by $s_i = -1$ with $n_i = \frac{1}{2}(1 + s_i)$, where s_i are scalar 'spins' (pointing up or down). Now all sites will interact and by rewriting $\mathcal{H}_{eff}$ with $\epsilon = 4J$ for the lattice gas we get:

$$\mathcal{H}_{eff} = \mathcal{H}_I - N(\frac{\epsilon}{2} + \frac{\mu}{2})$$

with the famous Ising Hamiltonian

$$\mathcal{H}_I = -J \sum_{\langle i,j \rangle} s_i s_j$$

where s_i is the spin value at site i and J is the *coupling strength* between two spins which here are equal for all sites.

Effective Hamiltonians arise for example in mean field theories where a many body problem is reduced to a one body problem. For the Ising model for example one can replace the spins in the Hamiltonian by fluctuations around the mean magnetization m (orientation) of a spin:

$$\mathcal{H}_I = -J \sum_{\langle i,j \rangle} s_i s_j - h \sum_i s_i = -J \sum_{\langle i,j \rangle} (m_i + \delta s_i)(m_j + \delta s_j) - h \sum_i s_i$$

If the fluctuations are small we can neglect the $\mathcal{O}(\delta s_i^2)$-terms and we can approximate the original Hamiltonian by an effective mean field Hamiltonian:

$$\mathcal{H}_I \approx \mathcal{H}_{MF} = 2Jm^2 N - \underbrace{(h + 4Jm)}_{h_{\text{eff}}} \sum_i s_i$$

where h_{eff} is an effective field of all the other spins acting on spin s_i. Thus we can describe an Ising system as if it consists of a single spin on which an external field acts. Since fluctuations are not negligible near a second order phase transition this formalism breaks down there (see *Ginzburg criterion* [28]).

With that we see the relation of the partition functions:

$$Z_{gas} = Z_I e^{\beta(\frac{\epsilon}{2}+\frac{\mu}{2})N} = Z_{\mathcal{H}_{eff}}$$

where Z_I is the canonical Ising partition function, Z_{gas} is the grand canonical partition function for the lattice gas and $Z_{\mathcal{H}_{eff}}$ is a partition function expressed with $\mathcal{H}_{eff}$. Thus we can model a box of gas particles equivalently by a spin lattice with different constrains which appear similar to an external field acting on the system.

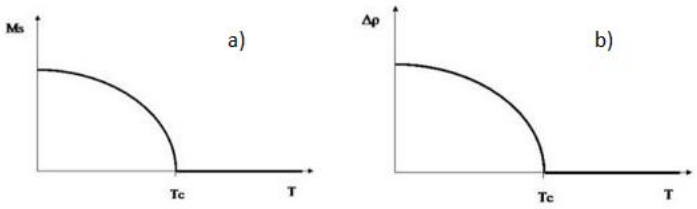

Figure 8: Corresponding phase diagrams and order parameters for a 2nd order transition. b) the difference in density ρ of distinct phases corresponds to a) the magnetization (the mean spin orientation). Figure adapted from [26].

The equivalence can be illustrated with the phase diagram of both models. The order parameter of the Ising model is the *magnetisation*, which is just the mean value of the spins at a given moment $m = \frac{1}{N}\sum_i s_i$ and for the lattice gas it's the particle's density $\rho = \frac{1}{N}\sum_i n_i$ (see figure 8). Both phase diagrams show a 2nd order phase transition; a discontinuity in the order parameter corresponds to a divergence in the second derivative of the free energy. Thus we see that we can break down complicated systems to their basic properties with spin lattices and still capture their thermodynamic phase behaviour.

The above can be extended to multi-component mixtures. But now we have to include all of the different interactions between the particles. As an example consider a binary mixture of species A and B [29]. The change in free energy has two contributions:

$$\Delta F_{mix} = \Delta U_{mix} - T\Delta S_{mix}$$

S_{mix} is the entropy of mixing and can be described by fraction of the mixture's components:

$$\Delta S_{mix} = -Nk_B(x_A \ln x_A + x_B \ln x_B)$$

where $x_A = n_A/N$ is the fraction which is occupied by A particles of total number n_A, for $x_B = n_B/N$ respectively. It is a concave function (see figure 9).

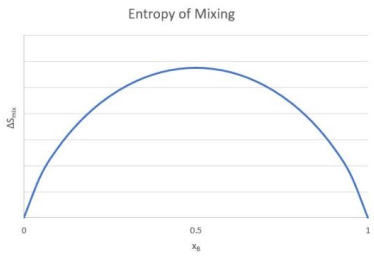

Figure 9: Entropy of mixing for a binary mixture of non interacting particles. Figure adapted from [27].

For a non-interacting gas (where $\Delta U_{mix} = 0$) this immediately gives the chemical potential of inserting a particle A:

$$\mu_A = \left(\frac{\partial F}{\partial N_A}\right)_{T,V,N_B} = -k_B T(\ln x_A - \ln x_B)$$

$$= -k_B T \sum_i \ln x_i$$

where the subscript indicated which quantities are held constant. In equilibrium the chemical potentials of all components have to match (then $dF = 0$).

For interacting particles the entropic term competes with the energy of mixing U_{mix}. We can introduce a χ-parameter which describes the energetic mismatch between particles A and B:

$$\Delta U_{mix} = U_{mix} - U_{pure,A} - U_{pure,B}$$

$$= x_A x_B N k_B T \chi_{AB}$$

where U_{pure} describes the energy of a pure liquid. $\chi_{AB} > 0$ for favourable A-B interactions and $\chi_{AB} < 0$ for unfavourable ones and the exact value defines their interaction strength. The total change in the free energy of mixing is then given by:

$$\Delta F_{mix} = N k_B T(x_A x_B \chi_{AB} + x_A \ln x_A + x_B \ln x_B)$$

For $\chi_{AB} > 0$ the free energy of mixing develops a maximum at low temperatures. This means that a system which exists in a mixed phase at high temperatures will eventually demix into two phases at low temperatures since the system always strives to minimize its free energy as we will see in the next part (see figure 10).

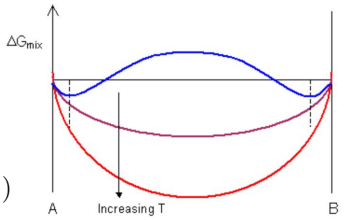

Figure 10: The Gibbs free energy of mixing as a function of the concentration of particles A and B for different temperatures T. As T is lowered the free energy develops a maximum. Figure adapted from [30].

2.4 Demixing

Demixing occurs e.g. due to a sudden temperature quench in systems undergoing a 2nd order transition. We can take the example of a binary mixture again (see section 2.3).

Above the critical point e.g. characterised by the critical temperature T_c the system is in a disordered phase. When cooled very rapidly small inhomogeneities, stemming from thermal fluctuations, persist and below the coexisting line the system ends up in an un-/metastable state and slowly distinct macroscopic phases form as the ordered domains 'grow' (see figure 11). Interfacial energy can slow the demixing down.

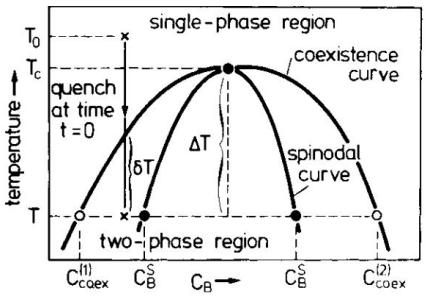

Figure 11: An isobaric (C-T) phase diagram of a system with a 2nd order phase transition. After a sudden temperature change (quench) crossing the coexistence curve, the system is found in a un-/metastable state. It will slowly demix over time depending on the miscibility gap. Figure adapted from [31]

As we have seen the free energy gets quite complicated when we add particles to a solution with different chemical interaction strengths (see section 2.3). For simplicity we will again focus on a binary (A-B) mixture; for $\chi_{AB} > 0$ at low temperatures this is depicted in figure 12. It can be seen as the overlap of two free energy curves of two pure substances. F' describes the free energy of the system as if it consists of a single phase and F represents the system consisting of two phases, each rich in A or B.

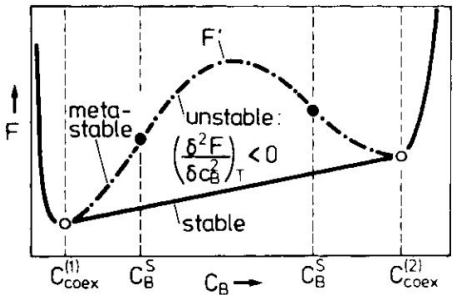

Figure 12: Free energy F as a function of concentration of species B. Meta- and unstable regions are shown depending on the behaviour of the 2nd derivative of F with respect to c_B. Figure adapted from [31].

When the system was in a mixed state and gets quenched and crosses e.g. the transition where it is described by demixed phases it is at first not in equilibrium. Non equilibrium processes are *irreversible* and it can be shown from the first law of thermodynamics (see eq. (1)) and $dS \geq 0$ that $(dF)_{T,V} \leq 0$ as the system relaxes towards equilibrium where $(dF)_{T,V} = 0$ [32]. From that also follows that the free energy of a system must be a convex function to be stable in equilibrium. Therefor the system is now in a state where we have two phases and their equilibrium free energy is given by a straight line connecting the pure states where F' has minima. One can find the equilibrium F by a *common tangent* construction. F is constructed by the *lever rule*, which states that one can find the equilibrium free energy of

intermediate concentrations by a weighted average (straight line) between the phase separated concentrations.

When we look at F' of such a system we get values for the concentration c_B (measuring with respect to B) where a single phase becomes unstable. The points where $\partial^2 F'/\partial c^2 > 0$ but $F' \neq F$ are called *metastable*; they are 'robust' to fluctuations but strive towards equilibrium by demixing. For a c_B inside this region one can always find a lower lying c'_B by a common tangent construction. In an isobaric phase diagram (see figure 11) the binodal or coexistence curve is defined by the line where the free energy differences between a one phase and two phase description match; the phases coexist. Here one starts to see distinct phases. Above T_c a 2nd order phase transition occurs as we have a single phase for any concentration.

For $\partial^2 F'/\partial c^2 < 0$ the system becomes *unstable*; any concentration fluctuations drive the system towards the demixed phases as fluctuations are related to 2nd derivatives of the free energy (see section 2.1). This defines the spinodal curve inside which long wavelength fluctuations (low energy temperature fluctuations) are sufficient to initiate the growth of ordered domains. Hence these regimes characterise the kinetics with which the system moves towards equilibrium.

2.5 Renormalization group

To get an understanding for universality we will look at the real space renormalization group from a block spin transformation point of view (see figure 13).

The idea of block spins was introduced by Kadanoff in 1966 [34]. Imagine a e.g. $2d$ spin system with nearest neighbour interactions. It is governed by a Hamiltonian which depends on many degrees of freedom (the spins) and a set of *coupling constants* $\{K_\alpha\}$ which define the interaction strengths. The lattice spacing a defines the smallest scale l on which fluctuations can occur. Now we apply a scale transformation by grouping spins in bigger blocks, for example $l' = 2a$. We can assign a new spin value to the coarsened block spin e.g. for the Ising model (where $s_i = \pm 1$) with the *majority rule*:

$$\tau(\sigma'_j, \{\sigma_i\}) = \begin{cases} 1 \text{ ,if } \sigma'_j = \text{sgn}(\sum_{i=1}^{b^d} \sigma_{j,i}) \\ 0 \text{ ,otherwise} \end{cases}$$

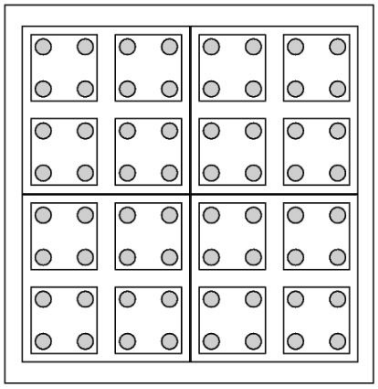

Figure 13: Sketch of a block spin transformation. The dots represent spins and are grouped into blocks of bigger and bigger size under $\mathcal{R}_b$. Figure adapted from [33].

Here d is the lattice dimension, b is the current block size and the spins are scalar. j indexes the coarsened blocks and i the spins in such a block. τ is called a *block spin projector* [35].

We already saw that at the critical point the system exhibits fluctuations on all scales; it becomes *scale invariant*. Macroscopic systems should be describable by renormalizable theories which should entail all phases of the system.

In terms of renormalization a scale invariant system is describable by a rescaled Hamiltonian which has the same form as the unscaled Hamiltonian but is described by a new set of rescaled coupling constants and a length scale $\mathcal{R}_b(K, l) \longrightarrow (K', l')$:

$$Z = \sum_{\{\sigma_i\}} e^{-\beta\mathcal{H}(\{\sigma_i\})} = \sum_{\{\sigma'_j\}} e^{-\beta\mathcal{H}'(\{\sigma'_j\})}$$

with

$$e^{-\beta\mathcal{H}'(\{\sigma'_j\})} = \sum_{\{\sigma_i\}} e^{-\beta\mathcal{H}(\{\sigma_i\})} \Pi_j \tau(\sigma'_j, \{\sigma_i\})$$

For renormalizable systems we are able to apply successive iterations of such scale transformations $\mathcal{R}_b\mathcal{R}'_b$ where $l' = bl$ and end up with a rescaled set that doesn't change anymore under $\mathcal{R}_b$. These are fixed points in *coupling space* and

describe critical points. At a fixed point one can linearly approximate the change in a coupling constant invoked by a change in a state variable (e.g. temperature or pressure). Some of the coupling constants grow under $\mathcal{R}_b$ (are **relevant**) while others shrink (are **irrelevant**). For example is the correlation length ξ a relevant variable as it diverges upon approaching T_c whereas the lattice spacing is an **irrelevant** variable. The behaviour of some coupling constants is not deducible from the linear approximation and they are called **marginal** (higher orders needed). The divergences are characterised by *critical exponents* which indicate the algebraic behaviour (see section 2.6), e.g. $\xi \propto \tau^{-\nu}$ where ν is the critical exponent.

With the block spin transformation we essentially integrate out the details of the system up to the correlation length ξ which are not needed to describe the macroscopic behaviour of the system in a certain state. After n iterations of $\mathcal{R}_b$ the correlation length behaves as $\xi(K) = b^{-n}\xi(K')$ which tells us that the correlation length must be infinite at the critical point. This makes the block spin picture intuitive.

Now we can understand the behaviour of F' of last section better (see section 2.4).

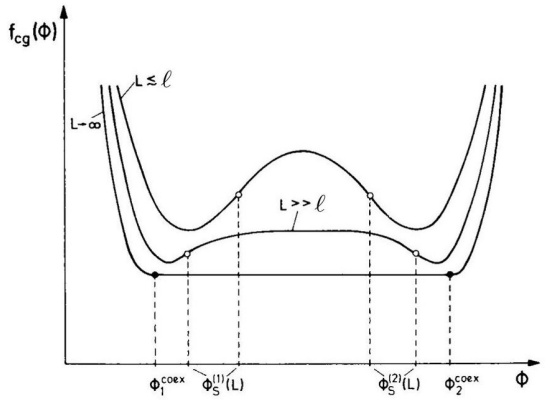

Figure 14: Coarse-grained free energy f_{cg} as a function of a rescaled concentration $\Phi = (c - c_{crit})/c_{crit}$ where c_{crit} describes the concentration at which the phases coexist. Here f_{cg} is taken to be symmetric (like in the Ising model). L is the coarse grained length scale and ℓ is the interfacial width stemming from e.g. fluctuations. Figure adapted and modified from [31].

In order to arrive at meaningful 'concentrations' from a lattice type approach we have to *coarsen* over lattice sites, since concentrations fluctuate discontinuously on the lattice spacing scale (think of two neighbouring sites with different particle types). Usually the scale up to which we coarsen L has to be small compared to the fluctuation scales which can not always be satisfied. We can introduce a coarse-grained ('mean-field type') concentration-gradient free energy f_{cg} (see figure 14) which describes the inhomogeneous mixture (thermal fluctuations) as a homogeneous phase (compare to section 2.4). The dependence of the

form of f_{cg} on the interfacial length scale ℓ is depicted in figure 14. The length scales at which the free energy describes a homogeneous mixture depends on the length scale of the coarsening L and on external conditions since fluctuation scales change upon approaching T_c. In the 'coexisting' region this coarsening is not valid if ℓ is smaller than L. As L is decreased the free energy landscape becomes more complicated than e.g. in a common tangent construction. The 'mean-field' approach can then be interpreted as an inaccurate description of the system where the coarsening is too rough. If this coarsening is valid on the other hand and we can do it for the whole lattice we will end up with a system where the mean field approach is valid.

In this sense many different looking systems actually can be described by the same Hamiltonian with rescaled coupling parameters. But note that renormalization is only possible if a fixed point exists in the first place. Its validity also depends on the spatial dimension. For example does the Ising model not have a transition in 1d (*lower critical dimension*, renormalising not valid) and for $d \geq 4$ its critical exponents coincide with exponents found in a mean-field description (*upper critical dimension*). If the number of neighbouring spins is large enough we can treat fluctuations as small since the ordering effect is stronger the more nearest neighbours a single spin has. For a regular lattice the number of nearest neighbours $\propto 2d$.

Not every Hamiltonian is renormalizable and the ones that are can be grouped into symmetry groups. The Ising model is invariant under the $Z(2)$ symmetry and many system fall into that symmetry group. The order parameter, the total magnetization, can be seen as capturing a spontaneous symmetry breaking of the system at a critical point. Below T_c the $Z(2)$ symmetry of the Ising model is broken as the system becomes ordered. The types of symmetries a system posses can be used to determine the universality class it belongs to as these Hamiltonians will have the same critical exponents for their divergences.

Therefor the lattice dimension (which depends on its geometry), the order parameter dimension and its symmetries are sufficient to distinguish between different universality classes.

2.6 Finite Size Scaling

When modeling thermodynamic systems, like spin lattice systems, we are not able to simulate them in the thermodynamic limit due to limited computer power and time. Instead we want to be able to deduce the behaviour of an infinite system through the simulation of finite systems and observe how it changes when we change the system size. This is necessary since the true thermodynamic behaviour only exists in that limit as finite size effects can mask the behaviour. By understanding finite size effects one can understand the behaviour in the limit. We will focus on 2nd order phase transitions.

As mentioned before for a 2nd order transition the important regime to study is in the vicinity of the critical point as the behaviour there characterises a system (see section 2.5). We saw that the correlation length ξ diverges and response functions can have singularities in the thermodynamic limit.

Observables for lattice systems can be defined on the basis of statistical moments of the spins which is evident from the relation of the partition function to e.g. the free energy $F = -k_B T \log(Z)$. From F we can derive observables by differentiation (see section 2.1).

The correlation function is related to the covariance of spins:

$$G(s_{00}, s_{r_x r_y}) = \left\langle s_{00} s_{r_x r_y} \right\rangle - \left\langle s_{00} \right\rangle \left\langle s_{r_x r_y} \right\rangle$$

where s_{00} is a reference spin and (r_x, r_y) is the distance to that reference spin on a $2d$ grid. From the correlation function the correlation length can be calculated which is usually done by fitting the correlation function since its behaviour is phase depended. For $T \neq T_c$ we have usually an exponential (fast) decay of correlations $G(r) \propto e^{-r/\xi}$ and for $T = T_c$ we have fluctuations on all length scales and an algebraic (slow) decay $G(r) \propto r^{-d+2-\eta}$, where d is the spatial dimension, η is the critical exponent for the correlation function and $r := |\vec{r}|$. The susceptibility is related to spin fluctuations and therefor to the 2nd spin moment as well as to the correlation function:

$$\chi = \frac{1}{k_B T} \left(\left\langle s_{ij}^2 \right\rangle - \left\langle s_{ij} \right\rangle^2 \right) \propto \int d^d r G(r)$$

Hence χ must also show an algebraic divergence at T_c. Also the other response functions behave algebraically near T_c as they are related to fluctuations. Most commonly the *reduced* temperature $\tau = \frac{T - T_c}{T_c}$ is used to describe the divergence to highlight the behaviour close to the critical temperature T_c at which the transition occurs.

Due to the finite lattice size the divergences e.g. of the correlation length is now limited; a finite size effect. This alters the critical behaviour, e.g. it shifts T_c. To make the transition from finite systems to systems in the thermodynamic limit we will use the susceptibility as an example. In the thermodynamic limit it diverges as $\chi(T) \propto \tau^{-\gamma}$ with critical exponent γ. Since the correlation length also diverges as $\xi \propto \tau^{-\nu}$ with critical exponent ν we can rewrite $\chi(T) \propto \xi^{\frac{\gamma}{\nu}}$. We now introduce a scaling function $\Phi(L, \xi)$ which takes care of the finite size

effects and recovers the correct behaviour in the thermodynamic limit. L is the system size and ξ again the correlation length and at the critical point this function can only depend on the finite system size L and ξ. The lattice spacing becomes irrelevant as the details of the system should not matter. Also we have fluctuations on all length scales and no intermediate length scale should therefor be 'special'. The behaviour χ_L for finite L can then be described as:

$$\chi_L(\tau) \propto \xi^{\frac{\gamma}{\nu}} \Phi(L/\xi)$$

$\Phi(L/\xi)$ recovers the correct limits: **1** if $L \longrightarrow \infty$ or the system is far from criticality $\Phi(L/\xi) = \text{const.}$ and we just end up with $\chi_L(\tau) \propto \xi^{\frac{\gamma}{\nu}}$. **2** If L is finite and $\xi \propto L$ (critical), $\Phi(L/\xi) \propto (L/\xi)^{\frac{\gamma}{\nu}}$ such that $\chi_L(T) \propto L^{\frac{\gamma}{\nu}}$. To highlight the behaviour with system size the relation is usually written in the form

$$\chi_L(\tau) = (L/\xi)^{\frac{\gamma}{\nu}} \tilde{\Phi}(L^{-\nu}\tau^{-\nu})$$

Thus we can extrapolate the behaviour in the thermodynamic limit from finite systems through *rescaling*. In a rescaling procedure observables (e.g. the susceptibility) can be plotted for different sizes and after rescaling the graphs with the scaling function and the critical exponents all the curves fall on top of each other (see figure 15).

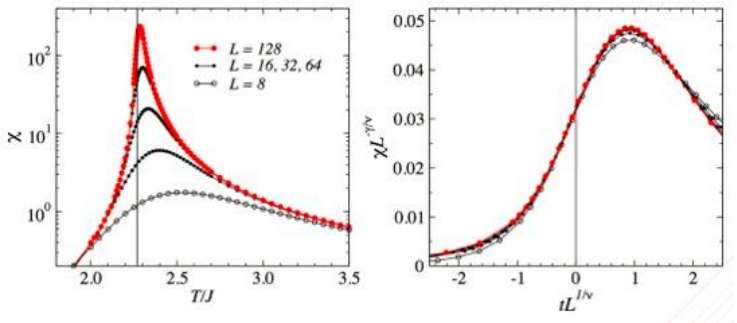

Figure 15: Susceptibility χ_L extracted for different system sizes and temperatures crossing T_c for the 2d Ising model. After rescaling the x and y axis with the critical exponents (for 2d Ising: $\gamma = 7/4$, $\nu = 1/4$) the curves collapse and thus the underlying system indeed behaves like a 2d Ising model near a 2nd order phase transition. Figure adapted from [36]

Systems with the same critical exponents are grouped into *universality classes*. For example we have seen that a system of gas particles belongs to the Ising universality class. The critical exponents can be calculated with the renormalization group flow and hence a universality class is deeply connected with the symmetries of the Hamiltonian by which it is described.

2.7 Continuous Fields

In this work we look at lattice systems with continuous spin distributions which I want to shortly introduce. We look at systems with continuous N-dimensional rotational symmetry $O(N)$ and translational symmetry (invariance under a shift $s_i \longrightarrow s_i + a$, with $a \in \mathbb{R}$).

The spin space of models with $O(N)$ symmetry is given by N-dimensional unit vectors:

$$\Omega_{O(N)} = \{\vec{s} \in \mathbb{R}^N : ||\vec{s}|| = 1\}$$

The interaction hamiltonian is given by the scalar product of neighbouring spins:

$$\mathcal{H}_{O(N)} = -J \sum_{\langle i,j \rangle} \vec{s_i}\vec{s_j} \tag{3}$$

where J is some interaction strength which we will take to be independent on grid location. For $J > 0$ spins favour to align.

For this work we are interested in the case $d = 2$. For $N = 1$ the Hamiltonian above (eq. (3)) corresponds to the 2D Ising model.

As we will need it later I want to mention the case $N = 2$ explicitly.

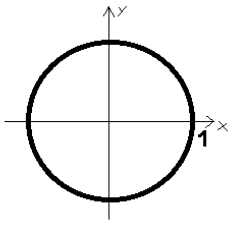

Figure 16: The spin space of the 2d XY model.

For this case eq. (3) is called the **2d XY model** which was studied intensively by Berezinskii, Kosterlitz and Thouless (short BKT) [37]. The spins live on a unit circle (see figure 16). In contrast to the Ising model this system has a $2d$ order parameter e.g. $\vec{m} = (m_x, m_y)^\perp = \langle \vec{s} \rangle$ and since it belongs to the $\mathcal{O}(2)$ symmetry group it is in another universality class.

It can be shown for the $1d$ and $2d$ case with $N \geq 2$ that there is no finite order phase transition. This is summarized by the *Mermin-Wagner theorem* [38]:

"*A continuous symmetry cannot spontaneously be broken at any finite temperature for systems with $O(N)$-symmetry with $N \geq 2$ and short range interactions (e.g. nearest neighbour-interactions) in $d = \{1, 2\}$.*"

Continuous symmetries are more 'robust' than discrete symmetries in the sense that it is harder to break them (see Ising model transition where $N = 1$ (discrete symmetry)).

Intuitively one can understand this by looking at a snapshot of a simulation of the $2d$ XY model at low temperatures (see figure 17).

To illustrate the concept fixed boundary conditions where chosen. At high temperatures the spins will be disordered and point in all directions due to the high thermal energy. At low temperatures the spins do not fully order but have quasi long range order: the 2-point correlation function decays algebraically

$$\langle \vec{s_i}\vec{s_j}\rangle = \langle \cos(\theta_i - \theta_j)\rangle \approx |i-j|^{-C/\beta}$$

for some $C > 0$. θ_i is the angle of spin i to some reference axis. At low temperatures neighbouring spins will point in roughly the same direction and one can approximate $\cos(\theta_i - \theta_j) \approx 1 - \frac{1}{2}(\theta_i - \theta_j)^2$. For $N > 2$ the correlations decay exponentially fast for any $T > 0$ [39], although this is debated e.g. for the **Heisenberg model** with $N = 3$ [40].

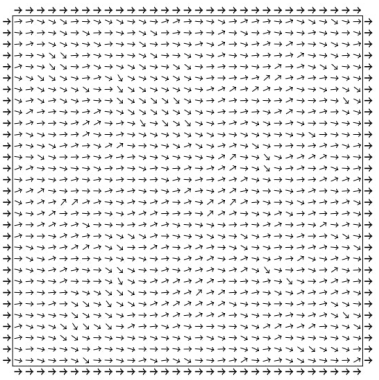

Figure 17: Simulation snapshot of the $2d$ XY model at low temperatures with fixed boundary conditions. The spins do not fully order but have quasi-long range order. Figure adapted from [38].

The absence of true long range order is due to the continuous symmetry: neighbouring spin deviations contribute with arbitrarily low energies.

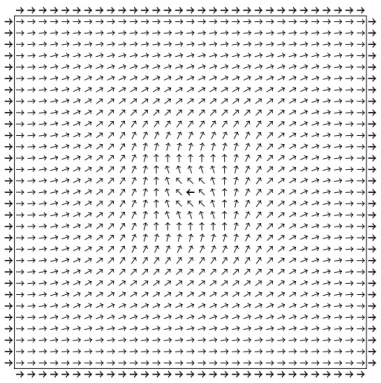

Figure 18: Ground state of the system for an enforced flipped spin in the centre. Figure adapted from [38].

In figure 18 a spin is flipped in the middle of the grid and it can be shown that the contribution to the Hamiltonian has an upper bound $\Delta\mathcal{H} \leq \frac{8C\beta\pi^2}{\log(1+N)}$ where $C > 0$ and N is the total number of spins [38]. It can be derived by a Taylor expansion of the potential energy V between two neighbouring spins: $V(\theta_i - \theta_j) \approx V(0) + \frac{1}{2}C(\theta_i - \theta_j)^2$, where $V'(0) = 0$ since V is symmetric. The angle is a continuous variable here and the angle difference (enforced by the boundary) vanishes as $N \longrightarrow \infty$. These *spin waves* prevent any long range order at finite temperature and no finite order phase transition can occur in the thermodynamic limit.

The XY model is quite complicated and exhibits a topological phase transition, the BKT phase transition. It describes the (un-)binding of vortices and is of infinite order; but will not be of relevance here.

Last I want to mention **gradient models** and keep the discussion to scalar spins. These are models where the Hamiltonian is continuously translational invariant since they only depend on neighbouring spin value differences. As it

will be useful later we consider as an example the *Gaussian gradient model* (or *Gaussian free field*) which is given by the Hamiltonian:

$$H_G = J \sum_{\langle i,j \rangle} (s_i - s_j)^2 + r \sum_i s_i^2$$

The sum runs again over nearest neighbours and the spins are scalar values. The term r keeps the spins bound to finite values. All terms are quadratic and thus the modes decouple in fourier space and this model is exactly solvable (see section x). For $r = 0$ the spins become unbound and can take on very large values. The variance of a spin diverges as

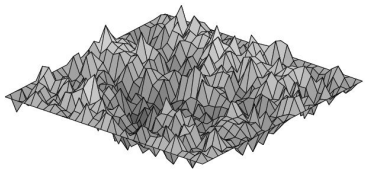

Figure 19: Example of a configuration of the Gaussian gradient model with boundary condition $\nu = 0$ for a 30x30 grid. Figure adapted from [38].

$$\sigma^2(s_0) \propto \begin{cases} L \text{ ,in 1d} \\ \log(L) \text{ ,in 2d} \end{cases}$$

where L is the system size. For $r \neq 0$ the correlations decay exponentially fast for all $T > 0$. Without the penalty term $\propto r$ one would not be able to define Gibbs measures for $d = \{1, 2\}$.

For dimensions $d \geq 3$ the number of neighbours is high enough such that $\sigma^2(s_0)$ becomes bounded even for $r = 0$. The correlations decay slowly as $G(s_0, s_r) \propto r^{-(d-2)}$ (here $\eta = 0 = \eta_{MF}$) and the susceptibility becomes infinite [38].

3 Biological Background

We have a general interest in the understanding of a complex membrane of many components and of finite size. To establish a connection to cell membranes I want to introduce some biological aspects of membranes. We orientate our simulations along Giant Plasma Membrane Vesicles (GPMV) experiments which I shortly want to introduce.

3.1 The Plasma Membrane

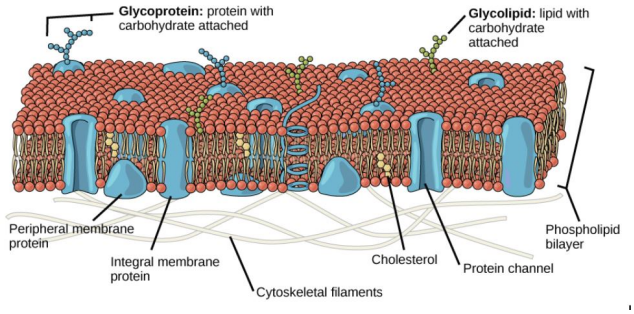

Figure 20: Sketch of an eukaryotic plasma membrane. Lipids (red/brownish) form the basic bilayer sheet by hydrophobic interactions in which proteins (blue) and cholesterol (yellow) are embedded. Such a membrane consists up to 50% of lipids, around 20-50% of sterols and of around 30% of proteins (by weight). The exact composition can vary drastically between different cells. Also shown is the cytoskeleton which runs along the cytosolic leaflet. Figure adapted from [41].

The interior of an eukaryotic cell (cytoplasm) is separated from the environment by the plasma membrane (see figure 20) and is embedded in a liquid (mostly aqueous) solution. Up to 50% of the plasma membrane are lipids (by weight). Lipids consists of usually two hydrocarbon chains attached to a polar headgroup (see figure 21). The bilayer structure of a membrane forms by 'polar' forces which let lipids spontaneously phase separate. In a bilayer the polar heads shield the apolar lipid tails from the water which minimizes the free energy. There are many different types of lipids in a plasma membrane which

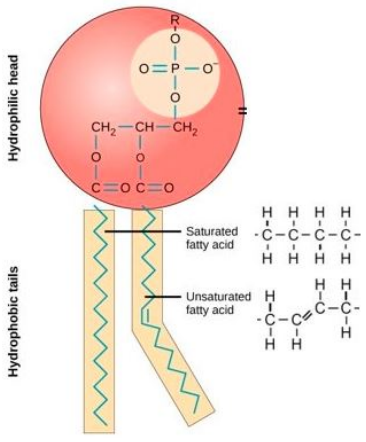

Figure 21: Example of a typical plasma membrane lipid, here a phospholipid. They are amphiphile molecules: they posses a hydrophilic headgroup (red) and a hydrophobic tail (yellowish). The tail consists of two hydrocarbon chains which can be different making the lipid asymmetric. They can be fully saturated (only single C-C bonds) or have unsaturated positions (double C=C bonds). A double bond creates a kink in the chain and makes lipids with many unsaturations floppy. Figure adapted from [41].

differ by their headgroup and tail length or saturation level. While their headgroups can differ substantially to fulfill many functions we just want to focus

on the tail. The carbon chains can differ in saturation levels, tail length (12-24 C-atoms) and saturation position. These considerations alone yields around $\mathcal{O}(10^2) - \mathcal{O}(10^3)$ distinct lipids.

Embedded in that bilayer sheet are many different types of molecules like proteins and sterols (see figure 20). We will come back to the role of proteins in the outlook and for now look at the most important sterol for animal cell membranes: cholesterol. These are rigid and bulky molecules made up of cyclic apolar hydrocarbon chains and an attached polar group (see figure 22). It's bulky hydrophilic part sits in between the spaces of the lipid tails making the membrane more rigid and allows for the control of membrane fluidity [42].

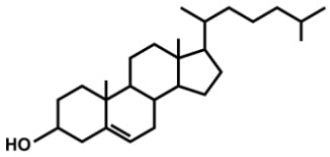

Figure 22: Structure of the most abundant eukaryotic cell membrane sterol: Cholesterol. The hydrocarbon rings give it a bulky and rigid shape and make it mostly unpolar except for the OH 'headgroup'.

If we consider a simplified membrane of only lipids and look at a single sheet of the bilayer (see figure 23) we see that unsaturated lipids occupy more space due to their kinks. They strive towards regions where they have a lot of space such that their configurational entropy maximizes. On the other hand saturated lipids have straighter tails which have stronger Vander-Waals attraction and they can come closer together. Unsaturated lipids are identified with a high melting temperature T_m and saturated lipids with low T_m. Together with cholesterol in ternary mixtures they show phase separation into liquid ordered (rich in cholesterol and low T_m molecules) and liquid disordered phases (high T_m rich) [4].

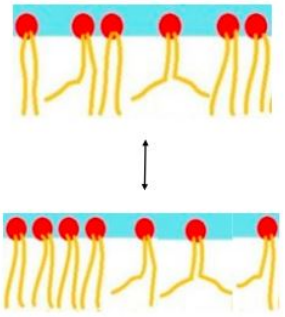

Figure 23: A monolayer of a lipid membrane. Lipid phases coexist (top) and lipid phase separation into liquid ordered and liquid disordered phases (bottom). Figure adapted and modified from [43].

In the liquid ordered phase cholesterol can fit in between the gaps of the saturated lipid tails to further magnifying the attractive forces. This suggests that the phase behaviour of a cell membrane is affected by the concentration proportion of saturated and unsaturated lipids (see section 2.4).

The complex chemical space creates a complex phase behaviour of the overall membrane in cells. In a constantly changing environment the membrane has to retain the right composition to guarantee unobstructed cell functionalities and its composition is constantly regulated [1]. I also want to mention that the two leaflets are asymmetric in compositions and by a process which burns ATP, components can be interchanged or pumped between leaflets with flippases from the inner to the outer leaflet [44]. This adds another level of complexity to the plasma membrane. Furthermore the membrane is attached to the cytoskeleton which creates non-diffusive points in the membrane.

3.2 GPMV experiments

In this work we are interested in studying the phase behaviour of a complex membrane of finite size. Cells are not macroscopic thermodynamic systems but micron-sized ($\approx 10 - 100\mu m$). Giant Plasma Membrane Vesicle (GPMV) experiments give insights into cell phase behaviour.

We saw in section 3.1 that research regarding plasma membrane phase behaviour was often conducted with ternary mixtures and their limitations.

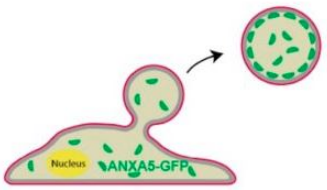

Figure 24: Sketch of a GPMV extraction. Functioning cells are grown at a temperature T_0 and vesicles are extracted which are fixed in composition. Figure adapted and modified from [46]

With the introduction of GPMVs a more accurate cell membrane composition can be achieved [45]. These are vesicles ($5 - 20\mu m$ in diameter) which are directly obtained by vesiculation from living cells, grown at a certain temperature T_0 (see figure 24). During this process the leaflet asymmetry gets lost and the vesicles have no cytoskeleton. They have no intracellular processes which together with the accurate cell composition makes them good toy models to study cell membrane phase behaviour. When they get cooled 10-15K below T_0 they spontaneously phase separate which is observed through optical fluorescence microscopy (see figure 25) [47].

By measuring e.g. the structure factor or the line-tension and averaging over a number of GPMVs (ensemble average) critical exponents were extracted which suggest that the demixing is critical and belongs to the 2D Ising universality class [3]. Upon changing the cell growth temperature T_0 the cell 'adapts' the composition of its membrane (as it is regulated) such that it always phase separates 10-15K below T_0. This suggests that cells are close to a critical point (see figure 26) and actively controlling their composition to remain 'critical'.

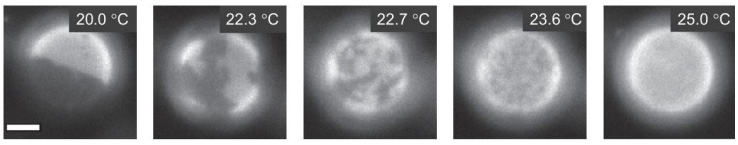

Figure 25: A GPMV extracted at $T_0 = 25°C$ and then slowly cooled down to $20°C$. A demixing into two phases is observed with fluorescent imaging with a critical point $T_c \approx 22.7°C$. The length scale (white) is $5\mu m$. Figure adapted from [47].

Many open questions arise. For example is it unclear if the cell membrane's phase behaviour gets altered by the GPMV extraction. Furthermore is it unclear how to reproduce the extraction procedure in simulations and do finite size scaling to extract critical exponents.

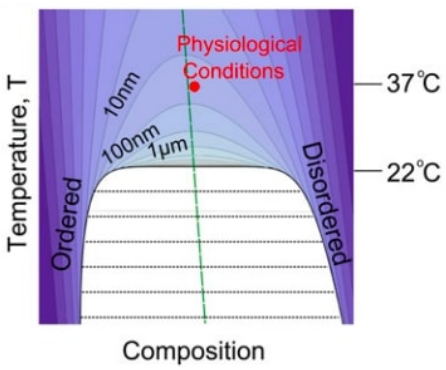

Figure 26: Cell membranes could be tuned close to a critical point a physiological conditions (red). The Ising isobaric phase diagram with the miscibility gap is shown. Below the critical temperature the membrane phase separates into a liquid ordered and liquid disordered phase. The contours indicate regions of constant correlation lengths. Figure adapted from [48].

It is not clear how a cell can maintain a critical composition (a composition that demixes when fixed and cooled). It would require a fine tuning of its composition which would require a sophisticated regulation mechanism. The exact cell composition also varies for individual cells during their lifetime, for example through dietary changes [49]. This suggests a manifold of 'critical compositions'.

4 Methods

4.1 Metropolis algorithm

To simulate lattice models we have to generate many microstates of the system to obtain statistical information about the thermodynamics. Here we employ a Metropolis algorithm to generate the states. Through iterated Markov Chain Monte Carlo (MCMC) steps we approximate the Boltzmann distribution of the system. A Markov Chain takes a microstate of a system, which is defined by a set of variables X to another microstate characterised by X', where the probability of a transition only depends on the current microstate and is independent of all other previous microstates 'visited'. A Monte Carlo step can be used in many ways but first I want to talk about the basic idea of Metropolis sampling [50].

We want to sample a collection of states based on an arbitrary distribution, which describes a thermodynamic ensemble in equilibrium; lets call it P(X), where X is a microstate of the system. In equilibrium P(X) is stationary and we have the *detailed balance* condition:

$$\frac{w(X' \longrightarrow X)}{w(X \longrightarrow X')} = \frac{P(X)}{P(X')} \tag{4}$$

where $w(X \longrightarrow X')$ is the weight of going from state X to X'. In equilibrium all processes are *reversible* and going from X to X' is equally probable as going from X' to X.

The Metropolis approach is now to sub divide the transition from one state to another into two steps:

$$w(X \longrightarrow X') = w_{acc}(X \longrightarrow X')A(X \longrightarrow X')$$

where w_{acc} is a proposal step which e.g. flips a spin and creates a new state X' with a new probability. This new configuration is then accepted based on some criterion which is described by the acceptance ratio $A(X \longrightarrow X')$. Inserting this into the detailed balance equation (eq. (4)) leaves us with:

$$\frac{A(X' \longrightarrow X)}{A(X \longrightarrow X')} = \frac{P(X')w_{acc}(X \longrightarrow X'}{P(X)w_{acc}(X' \longrightarrow X)}$$

There are different choices for the acceptance ratio. The Metropolis choice is either $A(X \longrightarrow X') = 1$ or $A(X' \longrightarrow X) = 1$ leaving us with the criterion:

$$A(X' \longrightarrow X) = \min\left(1, \frac{P(X')w_{acc}(X \longrightarrow X')}{P(X)w_{acc}(X' \longrightarrow X)}\right)$$

For a canonical ensemble $P(X)$ is the Boltzmann distribution. The acceptance ratio will depend on the energy differences ΔU of the two configurations: $A'(X' \longrightarrow X) \propto \min(1, \exp(-\beta\Delta U))$. Thus if a configuration is energetically more favourable it will always be accepted.

The distribution of the visited states $X_0, .., X_t$ converges towards $P(X)$ as a stationary solution. Initially the distribution is very different from $P(X)$ but since a Markov chain only depends on the current state ('memory-less') it will explore all possible states. The probability of finding the system in a state X will eventually be given by $P(X)$. A Markov processes is therefor *ergodic*. If the stationary solution is reached the system is in equilibrium.

Once in equilibrium we calculate statistics through spin moments of configuration snapshots and average them.

If two states are separated by a large energy barrier this algorithm has trouble to efficiently sample the full distribution since states with high energy have a small acceptance ratio. For example will an ordered Ising-like system practically never go from a state where all $s_i = 1$ to $s_i = -1$ since the energy cost for flipping a spin is proportional $-4J$ (J is the interaction strength).

The Metropolis algorithm is a *local* algorithm: it e.g. goes through each lattice site and attempts to swap a spin value based on the Metropolis criterion. Then for critical phenomena *critical slowing down* is observed. At the critical point large scale fluctuations are present in the system and correlation times are increased. A local algorithm will have trouble sampling all the microstates efficiently (that is in a reasonable amount of time) and higher order moments become difficult to compute. Therefor one often employs accelerated algorithms to speed up the simulation.

4.2 Replica exchange

To speed up the simulations we use *replica exchange* which is an example of a *global* update [51]. Especially near a critical point *correlation times* τ are enhanced which causes *local* algorithms to take a long time to explore the full phase space. Fluctuations will need exponentially long to relax back to equilibrium since the system is highly correlated.

Replica exchange speeds up simulations by running N different copies of an ensemble at different temperatures T_N. They are separated by ΔT. We now have a set of replicas $\{X\} = \{X^1_{T_1}, ..., X^N_{T_N}\}$ where the upper index denotes the replica or *walker* index which is later needed for reweighting.

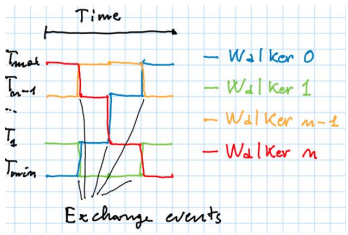

Figure 27: Sketch of walkers exchanging temperatures during the time of the simulation. Replicas from low temperatures eventually will be sampled at high temperatures as well. Figure adapted from [52]

It is more efficient to exchange the temperatures of the replicas and to rescale the energy like $E' = \sqrt{\frac{T_f}{T_0}}E$, where T_f and T_0 are the new temperature and the initial temperature respectively. Again we impose detailed balance:

$$P(\{X\})\omega(X \longrightarrow X') = P(\{X'\})\omega(X' \longrightarrow X)$$

where $P(\{X\})$ is the weight of the whole ensemble of replicas which is given by a product of the weights of each replica (see Metropolis algorithm).

We then find a Metropolis-like criterion to interchange the temperatures of two replicas:

$$A(1 \longrightarrow 2) = \min\left(1, \exp\left(\left[\left(\frac{1}{k_B T_1} - \frac{1}{k_B T_2}\right)(E_1 - E_2)\right]\right)\right)$$

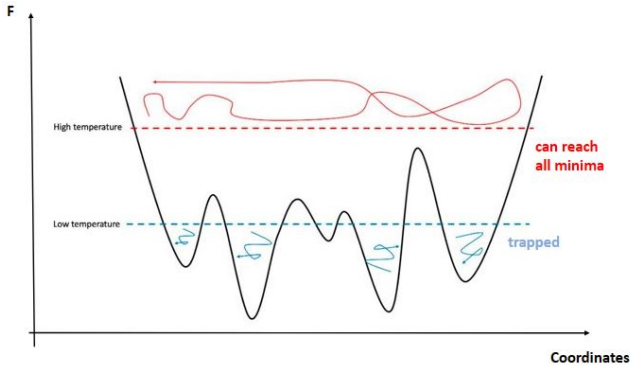

Figure 28: Sketch of replicas at different temperatures exploring a free energy landscape. Figure adapted from [53]

The acceptance rate is higher the smaller ΔT is but having more replicas also means higher computational cost.

By interchanging the configurations a system stuck in a free energy minima (e.g. low T) is able to overcome that barrier as its height effectively gets reduced at higher T (see figure 28). Similarly a system at high temperatures is able to relax and explore the 'valleys' of the free energy surface in more detail. Information on the kinetics get lost by implementing such algorithms.

4.3 Overcoming interfacial energy

To overcome interfacial energy in a demixing process (critical slowing down) we employ additional Gibbs frames (Gibbs ensemble MC) depending on the number of phase separations present [54].

An additional Gibbs frame introduces a copy of all replicas and now additionally two ensembles at same temperature can interchange particles/spins (see figure 29). When we consider a canonical ensemble of a binary mixture this will create two ensembles with opposite kind of species if the system demixes. In the current implementation the chemical potentials and volumes have to match in equilibrium and the particle number in each box is conserved. We do not impose equal pressure which is reasonable for large enough systems and symmetric spin distributions.

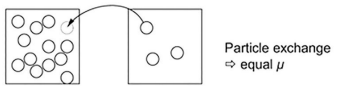

Figure 29: Sketch of the extra MC step used in Gibbs ensemble Monte Carlo. μ is the chemical potential. Figure adapted from [54].

Again we can come up with a Metropolis acceptance criterion for particle exchange and we have to impose that the boxes are now part of the grand canonical ensemble. If we try to insert a particle into box 1:

$$A_{\text{insert}}(1 \longrightarrow 2) = \min\left(1, \exp\left(-\beta\Delta U_1 + \ln\left(\frac{zV_1}{N_1+1}\right)\right)\right)$$

where z is the activity (which can be related to a χ parameter [55]), N_1 is the number of particles in volume V_1 of box 1 and ΔU is the energy change when a particle gets inserted. Note that we then also have to insert a particle into box 2 from box 1 in order to keep the particle number in both ('canonical') ensembles fixed. This is done by choosing the box of insertion/removal with equal probabilities which guarantees reversibility. The overall acceptance ratio is the product of the two processes, here for inserting a particle into box 1 and removing a particle from box 2:

$$p_{\text{exchange}} = p_{\text{insert},1} p_{\text{remove},2}$$

$$= \min\left(1, \exp\left(-\beta\left(\Delta U_1 + \Delta U_2 + Tk_B \ln\left[\frac{V_2\,(N_1+1)}{V_1 N_2}\right]\right)\right)\right)$$

and similarly for the other Gibbs frame.

4.4 Numerical implementation details

The code uses the C, C++, python and cuda languages and runs on single graphic card without parallelisation schemes [9]. We only employ lattice systems sizes of powers of 2 for convenience.

Simulations are performed in *semi-grand canonical* and *canonical ensembles*. Semi-grand canonical ensembles are often used in simulations of mixtures. The overall particle number of a system is fixed but different components are allowed to get exchanged for components on the grid (e.g. spin flips).

The canonical ensemble is simulated by constraining the spins of the semi-grand canonical ensemble. The constraint does not allow the spins to change their individual values anymore. They are now only allowed to diffuse on the lattice. We are not interested in the dynamics of a demixing process and to speed up the diffusion non-local MC moves are implemented. Instead of only swapping nearest neighbours, spins are exchanged up to a distance of $\ell = 2^l$ every time step, where $l < \log_2(L)$.

We will fix *periodic boundary conditions*, such that 2d lattice is wrapped upon a torus. Simulations were equilibrated with the number of MC sweeps depending on system size ($10^5 - 5 \cdot 10^6$ for equilibration) where the number of exchanges per sweep is $4L^2$. Statistics were taken every 4th sweep for $10^5 - 10^6$ sweeps. The code gathers the first four centered moments of different quantities like the spins, the spins with subtracted spatial mean, the magnetisation, the absolute magnetisation, the energy, ...

The autocorrelation function is a convolution of a signal with itself at different times. Here it is computed for every spin pair and with FFTs to reduce computational cost: $G(r) = \left\langle \mathcal{F}^{-1}\left(|\mathcal{F}(s(r) - \langle s\rangle_L)|^2\right)\right\rangle_t$ (see Wiener-Khinchin Theorem [56]), where $\langle s\rangle_L$ is the instantaneous spatial spin average. The FFT reduces the computational cost of a fourier transform $\mathcal{O}(L^2)$ to $\mathcal{O}(L\log(L))$ which is more efficient than calculating $G(r)$ with a convolution (which is also of $\mathcal{O}(2)$). For more details see 'Support information' of [9].

For single temperatures equilibration was done gradually: A system was initialised at a high temperature where it was allowed to relax before a slightly lower temperature was superimposed until the desired low temperature was reached. This was effective to avoid the system getting stuck e.g. in a vortex conformation in the XY model which takes a long time to relax. For parallel tempering the replicas ($\approx 64 - 256$) were spaced logarithmically to ensure effective swapping of replicas ($P(X) \propto e^{-\beta\mathcal{H}(X)}$).

For simulations the intern thinc-cluster of the MPI-P was used as well as the external TALOS cluster [57] were multiple simulations were run simultaneously on different graphic cards.

5 Previous Results

5.1 N-state 2D Ising model

The work in this thesis continues research conducted on a first model to describe a complex membrane of many components [9]. I therefor want to shortly introduce the model as well as mention some of the results. I will call it the N-state 2D Ising model which is given by the Hamiltonian:

$$\mathcal{H}_N = \chi \sum_{\langle i,j \rangle} |s_i - s_j| \tag{5}$$

The subscript N indicates the dependence on the number of available scalar spin states which are assigned as $s_i = \{-1, -1+2/(N-1), ..., 1\}$. The sum runs over nearest neighbours, $\chi > 0$ is some energy scale which defines the interaction strength (maximal energetic mismatch) and $\mathcal{H}_N$ is given in units of $k_B T$. For $N = 2$ this can be mapped onto the 2D Ising (ferromagnetic) model since the model conserves the $Z(2)$ symmetry of the Ising model. It is a gradient model and translational invariant (see section 2.7).

We are interested in the case $N \longrightarrow \infty$. As N increases one can imagine that a particle with slightly different interaction strength is added to the mixture where the individual differences become more subtle. As a simplified model for a cell membrane one can map the spins onto (a monolayer of) lipids with slightly different saturation (see section 3.1) where $s = -1$ represents a highly saturated lipid and $s = 1$ a highly unsaturated lipid. This choice reflects experimental results where unsaturated lipids phase separate from saturated lipids.

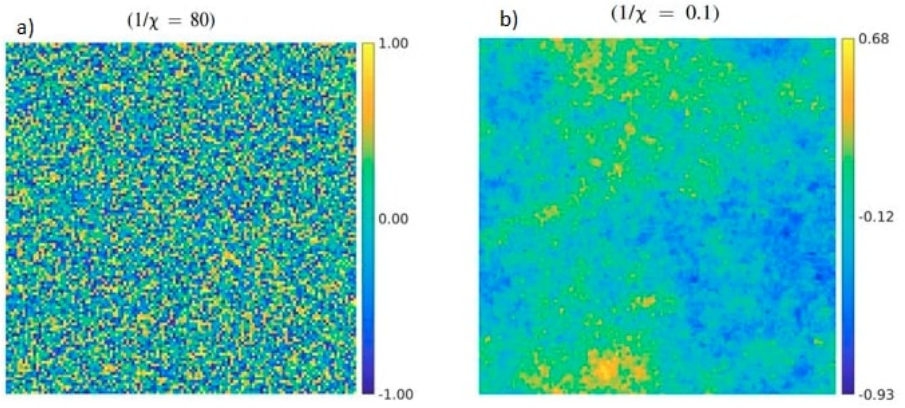

Figure 30: Snapshot of a $L = 128$ simulation in the limit $N \longrightarrow \infty$ at a) high temperature ($1/\chi = 80$) and b) low temperature ($1/\chi = 0.1$). Figure adapted from [9].

Figure 30 shows simulation snapshots at two different temperatures for this model in the limit $N \longrightarrow \infty$. At high temperatures the full spin space is sampled

uniformly and the system is completely disordered. At low temperatures we do not find a single ordered phase ($\langle m \rangle$ remains 0) but a quasi ordered phase and instantaneously only part of the spin space is sampled.

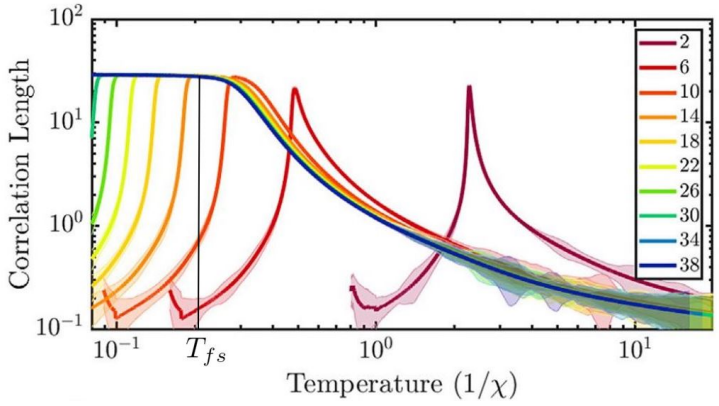

Figure 31: The correlation length as a function of temperature for a $L = 64$ system is shown where N is gradually increased from $N = 2$ to $N = 38$. The onset temperature is marked as T_{fs} for the case $N = 38$. Figure adapted from [9].

Figure 31 shows the correlation length as a function of temperature (translated to the energy scale χ) for a $L = 64$ system and increasing values of N. For $N = 2$ the usual phase transition peak in the correlation length is observed which corresponds to the *'critical temperature'* which is identified with the 2D Ising model critical temperature $T_{c,\text{Ising}}$ (for a finite system size). As N increases a plateau region over a temperature range manifests below an onset temperature T_{fs} which becomes independent of N if N is *sufficiently large*. For finite but large N the plateau region ends at $T_c \propto T_{c,\text{Ising}}/(N-1)$ (thus $T_c \longrightarrow 0$). The plateau persists down to $T = 0$ in the limit $N \longrightarrow \infty$. Finite systems display this feature already if N is sufficiently large (here for $N \geq 38$). A plateau region suggests system spanning correlation lengths over a range of temperatures $T_c < T < T_{fs}$ which is a departure from discrete systems. The correlation length divergence is limited by the finite system size.

In figure 32 N is set to be sufficiently large and L is varied. The plateau region vanishes as L increases; the onset temperature T_{fs} is a function of L:

$$T_{fs}^{-1} - \frac{1}{2}\log\left(T_{fs}\right) \approx 1.12\log(L) - 1$$

This suggest that the critical behaviour vanishes in the macroscopic (thermodynamic) limit and that the behaviour stems from finite size effects. For each size we have quasi long range order with system spanning correlation lengths below T_{fs}.

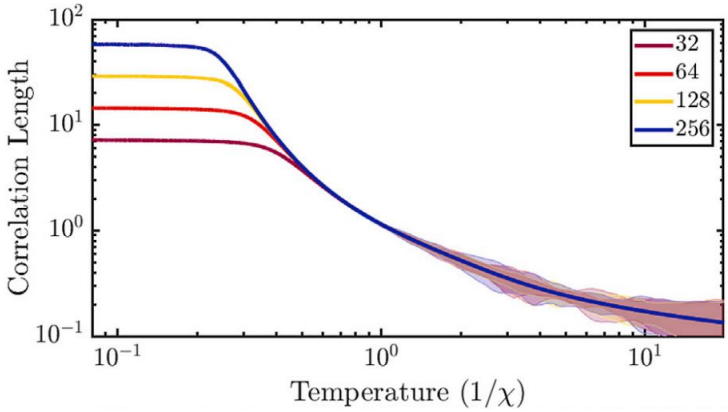

Figure 32: The correlation length as a function of temperature in the continuous limit where N is sufficiently large for different system sizes. Figure adapted from [9].

The spin space of the model can be visualized as in figure 33 where $\Omega(s)$ is the spin space density. At high temperatures a uniform distribution is sampled (black) and at low temperatures only a fraction of the spin space is instantaneously sampled (red) (see σ_L in figure 34). For low T the system acquires a translational invariance: the instantaneous sampled spin distribution is free to translate between -1 and 1.

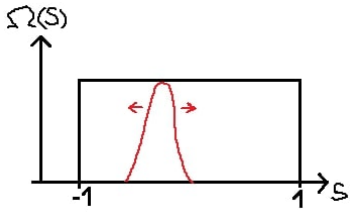

Figure 33: Uniform spin distribution underlying the N-state 2D Ising model. At high temperatures the full spin space is sampled at every instance whereas at low temperatures (red) only part of the spins space is sampled which drifts between $s = -1$ and $s = 1$.

To fully understand the hamiltonian we can explicitly include the chemical potential term from the semi-grand canonical simulation in the Hamiltonian (eq. (5)):

$$\mathcal{H}_N = \chi \sum_{\langle i,j \rangle} |s_i - s_j| - k_B T \sum_i \log \Omega(s_i)$$

$\mu_i = -k_B T \log(\Omega(s_i))$ is the chemical potential for spin value s_i based on a density of states which in this case is the uniform distribution which keeps the spins in the interval $[-1, 1]$. It generally follows from similar considerations as in the lattice gas section where a chemical potential appeared when describing the system in a grand canonical ensemble (see section 2.3):

$$Z_{GC} = \frac{1}{(2N+1)^K} \sum_{s_1=-1}^{1} \sum_{s_2=-1}^{1} \dots \sum_{s_N=-1}^{1} e^{-\mathcal{H}} \approx \int_{-1}^{1} \Omega(s_1) ds_1 \dots \int_{-1}^{1} \Omega(s_K) ds_K e^{-\mathcal{H}}$$

$$= \int_{-1}^{1} ds_1 \int_{-1}^{1} ds_2 ... e^{\ln \Omega(s_1) + \ln \Omega(s_2) + \cdots} e^{-\mathcal{H}}$$

where the sum contains $2N+1$ states, $K = L^2$ is the total number of spins and $\mathcal{H}$ is the interaction Hamiltonian (eq. (5)). This lets us again define an effective Hamiltonian:

$$\beta \mathcal{H}_{\text{eff}} = \beta \mathcal{H} - \sum_{i=1}^{N} \ln \Omega(s_i), \text{with} \int_{-1}^{1} \Omega(s) ds = 1$$

The chemical potential can be seen as an external field of entropic origin. In the N State Ising model we choose all states to be equally dense. Biologically speaking this can be seen as a lipid exchange/insertion mechanism that does not distinguish between different types of lipids.

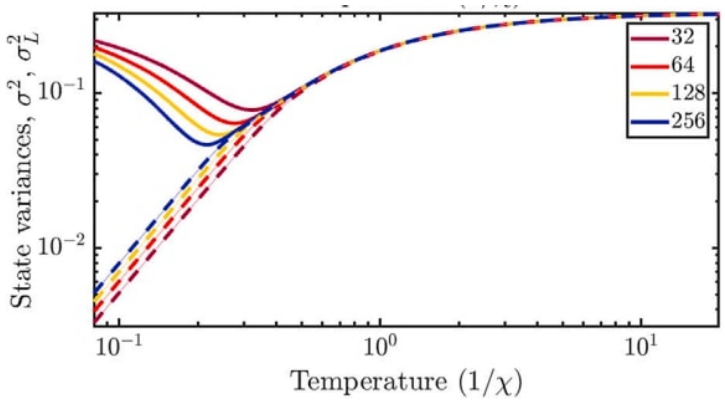

Figure 34: σ^2 and σ_L^2 are plotted as a function of temperature in the limit $N \longrightarrow \infty$ as a function of temperature. Below T_{fs} the quantities are unequal. Figure adapted from [9]

To get insight into the behaviour below T_{fs} the system is characterised by its spin distribution. Two different distributions are considered: a time averaged distribution $\mathcal{D}(T, s)$ and an instantaneous spatial averaged distribution $\mathcal{D}_L(T, s)$. They are related by $\mathcal{D}(T, s) = \langle \mathcal{D}_L(T, s) \rangle_t$ where $\langle . \rangle_t$ is a statistical time average. These distributions are characterised by their variances: the usual ensemble averaged variance $\sigma^2 = \left\langle \langle s^2 \rangle_t - \langle s \rangle_t^2 \right\rangle_L$ and the instantaneous *spatial* variance $\sigma_L^2 = \left\langle \langle s^2 \rangle_L - \langle s \rangle_L^2 \right\rangle_t$ which differ in the order in which the averages are taken and $\langle . \rangle_L$ is a statistical space average. Figure 34 shows the two variances as a function of temperature for different system sizes in the 'continuous' limit (for N sufficiently large). Due to the continuous nature of the model the system never fully orders as there are arbitrarily low energy excitations (see section 2.7). The instantaneous spin distribution becomes narrower than the available spin states as T is lowered. Below T_{fs} $\sigma_L^2 \propto T$ and $\sigma_L^2 \neq \sigma^2$. The thermal average can be decomposed into a spatial and a temporal average and the

order of taking them should not yield different results in thermal equilibrium. The discrepancy of these two quantities below T_{fs} means that 'macroscopic' thermodynamics is 'broken' in that regime: systems of finite size are not ergodic anymore. But as we saw, the behaviour vanishes for $L \longrightarrow \infty$, where also $\sigma^2 = \sigma_L^2$.

Since σ_L^2 becomes linear below T_{fs} one can take the fraction of σ_L^2 for different sizes in the linear regime. By doing so one finds an apparent scaling law whose origin we explore in this work:

$$\sigma_L^2(T_0) \propto L^{-0.2}$$

Lastly I want to mention that the finite size regime of the system was found to be qualitatively unaffected by the exact form of the chemical potential. Here we want to further explore if the behaviour is robust to other modifications to $\mathcal{H}_N$, e.g. like the changing the spin dimension. For further details on the system see [9].

6 Results

This work is divided into two parts. In the first part we will examine the 2D XY model to show that they behave similar to models of the type introduced in section 5 although we change the order parameter dimension. Secondly we approximate such models by an analytically solvable model. We then analyse it to find the origin of the apparent scaling law of section 5.

6.1 2D XY model analysis

6.1.1 Correlation length of the 2D XY model

The 2D XY model was introduced in section 2.7. One can rewrite the Hamiltonian

$$\mathcal{H} = -J \sum_{\langle i,j \rangle} \vec{s_i} \vec{s_j} = -J \sum_{\langle i,j \rangle} \cos(\theta_i - \theta_j)$$

Here we implement it using squared spin differences (with a uniform underlying distribution $[-\pi, \pi]$ for the angle θ):

$$\mathcal{H}_{XY} = J \sum_{\langle i,j \rangle} (\vec{s_i} - \vec{s_j})^2$$

This can be mapped onto the 2D XY model Hamiltonian introduced before:

$$(\vec{s_i} - \vec{s_j})^2 = \vec{s_i}^2 + \vec{s_j}^2 - 2\vec{s_i}\vec{s_j} = 2s^2 - 2s^2(\cos\theta_i \cos\theta_j + \sin\theta_i \sin\theta_j)$$

$$= \frac{1}{2}(1 - \cos(\theta_i - \theta_j))$$

where $\vec{s} = |\vec{s}|(\cos\theta_i, \sin\theta_j)$ with $|\vec{s}| \coloneqq s = 0.5$ and $\cos\theta_i \cos\theta_j + \sin\theta_i \sin\theta_j = \cos(\theta_i - \theta_j)$ was used. We can ignore the constant factor in the Hamiltonian. Thus $\beta'_{BKT} = \frac{1}{2}\beta_{BKT}$ where β'_{BKT} is the critical inverse temperature for our model for the BKT-transition and $\beta_{BKT} \approx 1.13$ [58] from the 2D XY model introduced in section 2.7.

First we reproduce the plateau plots for the correlation function of the 2D N-State Ising model. To do so we equilibrate 3 systems of different size with replica numbers depending on that size for an inverse temperature range crossing $\beta'_{BKT} \approx 0.565$. The correlation function is calculated by FFTs and averaged for every reference point on the grid (see section 4.4). A reference point on the grid was chosen and the correlation function was reduced to 1d by using the radial symmetry of the model:

$$G(\vec{s}_{00}\vec{s}_{xy}) \longrightarrow G(s_{00}s_{x0})$$

Note that due to the periodic boundary conditions only points up to $L/\sqrt{2}$ are independent.

The correlation length ξ was extracted by fitting an exponential $e^{-|x|/\xi}$ (with $x = (0, .., L/\sqrt{2})$) to the correlation function. ξ of a fit from the previous (higher) temperature was used as an estimate for the next fit. Note that at low T the exponential decay changes in the low temperature regime to an algebraic decay in the 2d XY model (quasi long-range order). We are only interested in the quantitative trend of the correlation length and by always fitting an exponential we still can observe the approximate course of ξ.

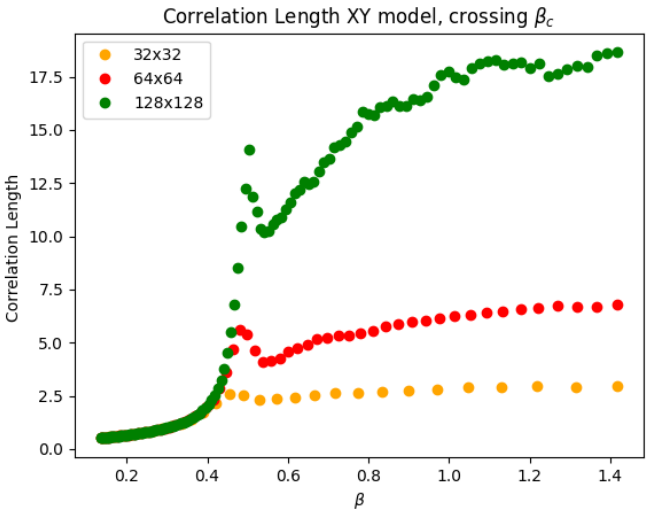

Figure 35: Correlation length over a range of inverse temperatures β for the 2D XY model, crossing β_{BKT}. The BKT-transition is visible with β_{BKT} approaching the value 0.565 as L increases. For high β the correlation length plateaus and reaches a characteristic value depending on system size. The label indicates different system sizes L.

Figure 35 shows the extracted correlation lengths for 3 different system sizes. In the low β regime (above the BKT-transition) the spins are uncorrelated (disordered phase) and upon lowering the temperature the correlation length increases (binding of vortices) until it reaches a peak which we identify with the BKT-transition temperature. Below the transition the correlation length first decreases (binding of vortices) and then starts increasing again before finally settling to a system size depending value. The onset for the plateau region (where the correlation length reaches its final value) appears to move to $\beta_{fs} \longrightarrow \infty$ for increasing system sizes. Thus the XY model displays a qualitative similar feature (finite size effect) as the 2D N-state Ising model with system spanning correlation lengths above β_{fs}.

A plateau region was found for the 2d Heisenberg model as well by P. Schmoll et al., but for extrapolations to infinite systems with a tensor network approximation (for details see [59], figure 7). Thus indicating that the behaviour found here could be extrapolated to even higher spin dimensions, although this needs to be shown explicitly for finite systems without approximations.

6.1.2 Patching Distributions - Simulating GPMV experiments

To imitate the GPMV experiment procedure we equilibrate a system in the semi-grand canonical ensemble by gradually cooling it down (setting a slightly lower temperature over the curse of 10^6 equilibration sweeps) until a temperature T_0 deep in the plateau region is reached. Then a switch from the semi-grand canonical to a 'canonical' ensemble is performed by fixing the spin values, allowing them only to diffuse on the lattice. MC moves do not attempt to replace a spin by a completely new one but only attempt to swap spin values on the grid (see section 4.4). For abbreviation I will refer to these spin distributions as 'constrained'. To be able to compare the spin distributions they were rotated after constraining such that $< s_x >= 0$ (where s_x is the x-component of spins). To overcome interfacial energy a second Gibbs frame was set up (see section 4.3) and the demixing was simulated by copying the equilibrated grid onto replicas (number depending on system size) around T_0. After another equilibration we extract statistical moments and calculate the susceptibility χ. When χ is plotted against the rescaled temperature T/T_0 we observe a peak in the susceptibility which we identify with a demixing temperature T_{demix} (see figure 36). We associate the plateau with a pseudo-critical regime; in that regime all properly equilibrated distributions show a demixing while for $T_0 > T_{fs}$ they do not (no peak in e.g. the susceptibility). It appears as if the system keeps the instantaneous spin variance narrow enough such that demixing can occur at any temperature for $T_0 < T_{fs}$. Interestingly the peak height is not diverging as L is increased.

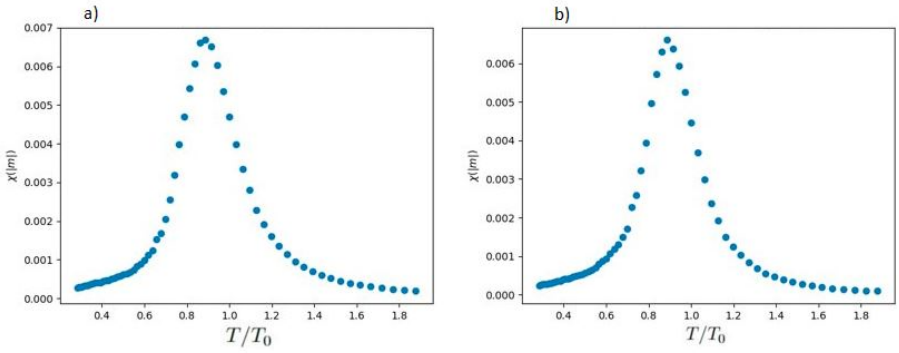

Figure 36: Example of a demixing transition for a) $L = 32$ and b) $L = 64$. The peak in the susceptibility is identified with the demixing temperature T_{demix}. $T_0 = 0.02$ for both systems. In all following plots only 1 of the Gibbs frames is shown since they are symmetric when looking at observables related to $|m|$.

We could now proceed by equilibrating systems of different sizes, cooling them down and extracting a critical exponent by finite size scaling. But due to the underlying continuous spin distribution the frozen spin distributions are always characterized by slightly different moments since we can have excitations of arbitrarily low energy (see section 2.7). The susceptibility peak position

sensitively depends on the underlying instantaneous spin distribution and is a stochastic variable.

The peak position also depends on system size and to do finite size scaling we take a small ($L_0 = 16$), equilibrated system, fix the spin values and patch its spins onto larger grids of size $L_0 \cdot 2^n$, where n is an integer ≥ 1, by multiplying the grid (and thus each spin) by 4^n (see figure 37). Although a distribution where 2 or more spins are identical would never be generated the (entropic) error by doing the patching is small ($\propto 4^n/L^2$). We then again distribute these grids onto an additional Gibbs frame and replicas and let the systems demix. Thus we constrain the instantaneous variance $\sigma^2_{L_0}$ for all grids to be that of a $L = 16$ system, allowing for finite size scaling. It is unclear if this procedure works in reverse though.

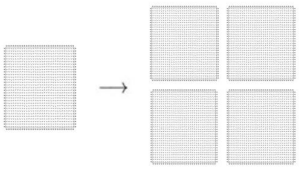

Figure 37: Sketch of patching procedure. Here for next biggest system size. Figure adapted and modified from [38].

The susceptibility peak height is largely unaffected by system size but the peak position moves towards lower T_{demix} with increasing system size, suggesting $T_{\text{demix}} = 0$ for $L \longrightarrow \infty$ (see Appendix). It is possible to collapse the peak position with an apparent scaling law $T_{\text{demix}}/T_0 \propto (L/L_0)^{-0.2}$ (see figure 38). Since the variance σ^2 decreases with system size we see that for the patched systems the imposed σ^2_L is slightly too small causing them to be further off criticality ($T_{\text{demix}} \ll 1$).

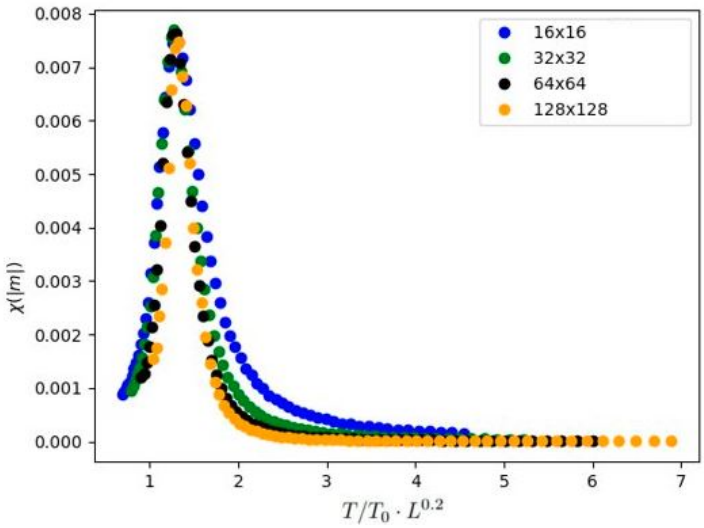

Figure 38: Rescaled susceptibilities for different system sizes. The peak position collapses for an apparent exponent -0.2 while the peak height is not rescaled. $T_0 = 1/30$ here.

To gain insight into what attributes of the spin distribution affect T_{demix} we go back to a single system size and let many of such systems demix. We then

fit the peak in the susceptibility by a Gaussian and extract the mean as a value for T_{demix}/T_0 and extract moments of the instantaneous spin distribution. If we plot T_{demix}/T_0 against σ_L^2 we find a linear dependence (see figure 39). Of

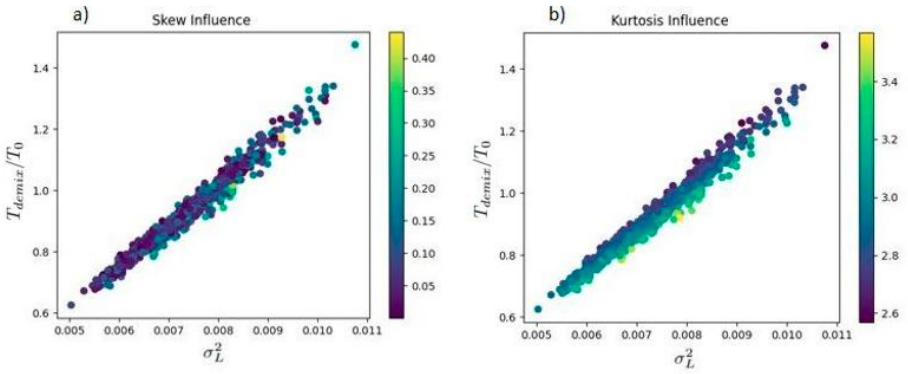

Figure 39: T_{demix}/T_0 plotted against σ_L^2 (instantaneous variance) for a $L = 64$ grid deep in the plateau ($T_0 = 0.02$) for ≈ 1000 simulations. The relation is linear and the slight influence of the kurtosis (b)) on T_{demix}/T_0 is shown while the skew (a)) has no influence.

the 4 moments σ_L^2 has the biggest impact on T_{demix}. The skew seems to have no impact on T_{demix}, although we do not have a pressure piston for the Gibbs ensemble updates (see section 4.3).

That is, the two Gibbs frames have identical volumes and a demixing results only in identical volumes if the fixed spin distribution is symmetric, but a skewed distribution is asymmetric. The dependence on the skewness could therefor be hidden. The higher the value of the kurtosis is the more tailed is a distribution. The kurtosis of the distributions suggests that they are roughly Gaussian and that spin distributions with less pronounced tails demix at higher temperatures than heavily tailed spin distributions. With the linear dependence of T_{demix} and σ_L^2 we find that the apparent exponent matches

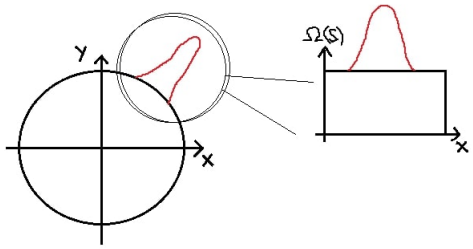

Figure 40: The spins in the XY model are 2 dimensional and uniformly distributed along the unit circle at high temperatures. At low temperatures only a part of the circle is sampled due to quasi long-range order.

$$\frac{T}{T_0} \propto \left(\frac{L}{L_0}\right)^{-0.2} \propto \sigma_L^2$$

the one which was found previously for the 2D N-state Ising model. If this is a real scaling law it would show that the order parameter dimension for finite sys-

tems below T_{fs} with many components does not affect the universal behaviour of the system, surprisingly 'breaking' universality as we know it from macroscopic thermodynamics since usually systems with different spin dimension belong to different universality classes.

We rationalize this by looking at the spin space of states of the 2D XY model (see figure 40). In the low temperature regime we have quasi long-range order which instantaneously breaks the rotational symmetry (only a fraction of the spin values is sampled) as the spins align along a common direction. Below T_{fs} the circle can locally be thought of as a 1D interval. We thus end up with a uniform spin state density $\Omega(s)$ as for the 2D N-state Ising model.

6.1.3 Attributes of spin distributions below T_{fs}

To see if the demixing is well behaved, T_{demix}/T_0 was extracted again. A histogram of the values was approximated by a kernel-density estimation (see figure 41).

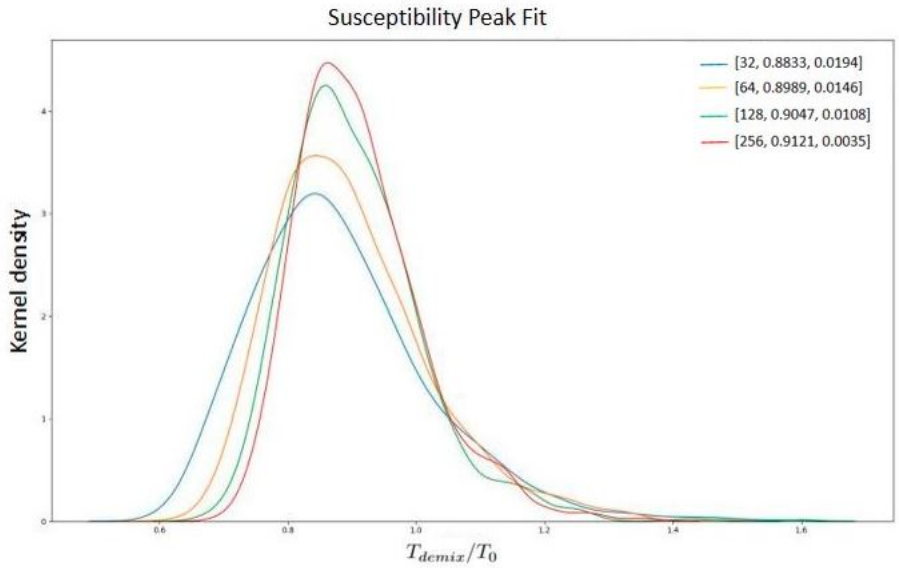

Figure 41: Kernel-density estimation of the extracted T_{demix}/T_0 values for ≈ 1000 values for each system size. The label shows [system size, mean, variance] of the distributions. Statistics are not good enough to tell whether the tail is an artefact of poor statistics.

The mean of the distribution appears to move towards $T_{\text{demix}}/T_0 \longrightarrow 1$ for $L \longrightarrow \infty$ suggesting that finite size systems are slightly 'off criticality'; an infinite system appears to be right 'on criticality' with $T_{demix}/T_0 = 1$ (then $T_0 = T_{\text{demix}}$). At the same time the distributions become narrower as L increases and seem to converge towards a delta function for $L \longrightarrow \infty$. In this sense the apparent critical demixing behaviour would be well behaved.

Since we have a linear dependence between T_{demix}/T_0 and σ_L^2 we only have to extract the moments of the equilibrated distributions before patching and identify σ_L^2 with T_{demix}/T_0 up to some proportionality constant. This drastically reduces the computation time (by more than 10 times) and it was now possible to extract moments from 10000 individual simulations. With this we increase the accuracy of the statistics describing the equilibrated spin distributions. The extracted instantaneous variances as a histogram are shown in figure 42 for a $L = 64$ system.

The distribution of σ_L^2 is well fitted by a Gamma distribution and the CDF shows that the tails of distributions are not an artefact of poor statistics (see Appendix). A potential source for a Gamma distribution is a (sum of) Gaussian

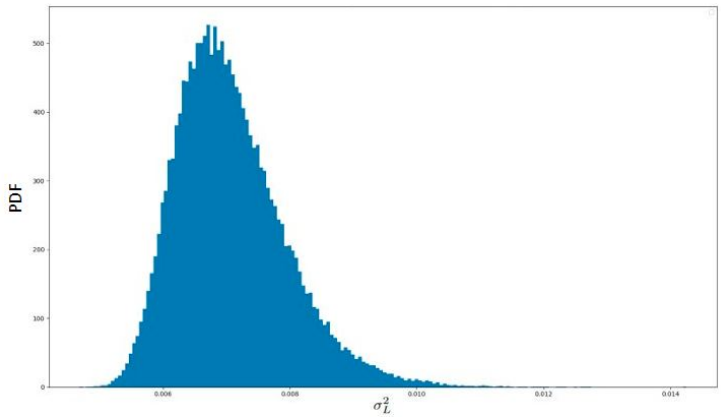

Figure 42: Histogram of σ_L^2 for the equilibrated spin distributions of a $L = 64$ grid for 10000 entries (at $T_0 = 0.02$).

distribution(s) squared:

$$N^2(0, \sigma_L^2) = \text{Gamma}(\frac{1}{2}, 2\sigma_L^2)$$

where 0 is the mean of the Gaussian and N stands for Gaussian distributed random variable. This can be seen e.g. for the Maxwell-Boltzmann distribu-

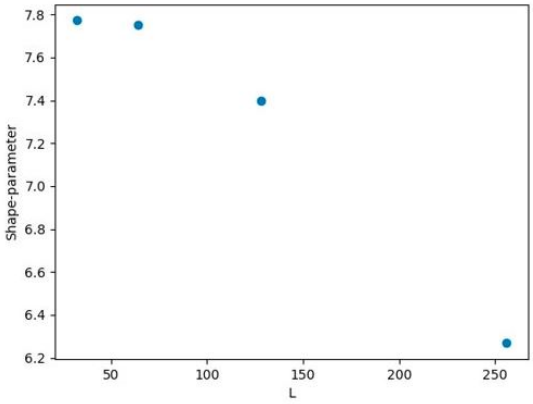

Figure 43: Shape parameter against system size of the Gamma distributions for different system sizes. The shape parameter captures how skewed the distribution is or how pronounced the tail w.r.t. overall distribution is (it regards the 'shape' of the distribution). It is therefor related to higher moments. Here again it suggests a convergence to a delta-function as L increases.

tion which is the distribution of the random velocities of particles squared in equilibrium. The sum of independent Gamma distributions is again a Gamma

distribution. This behaviour of σ_L^2 hints towards that the underlying instantaneous variances are Gaussian distributed random variables influencing T_{demix}/T_0 quadratically. But this will become more apparent in later sections of the results.

One can extract the parameters for the Gamma fits. Figure 43 shows the shape parameter, which decreases as L increases. It verifies that the tails contribute less to the histogram and it becomes more symmetric as L is increased.

6.2 2D FFT analysis

It would be really helpful to have analytical access to the apparent scaling behaviour of the observables, especially the instantaneous spin variance σ_L^2 where the peculiar $\frac{1}{5}$ apparent scaling exponent was observed. For simplicity we come back to scalar spin systems now.

An analytical solvable model would be a Gaussian-like model where the spins enter the Hamiltonian quadratically since the modes then decouple in fourier space. Therefor, for squared interactions, we qualitatively tested the behaviour of σ_L^2 at low temperatures for different underlying spin distributions (see figure 44).

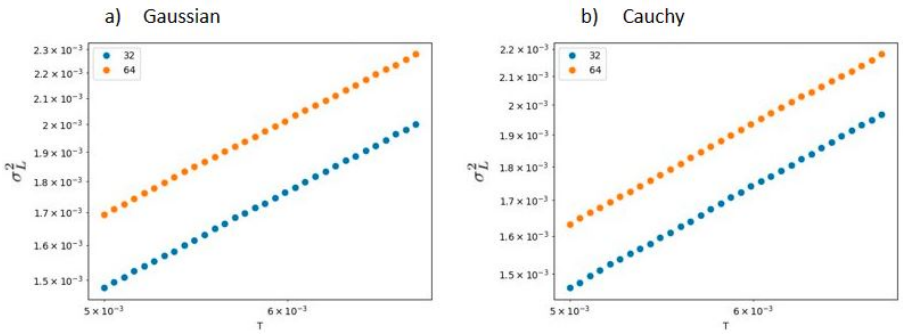

Figure 44: σ_L^2 for low T for a) a Gaussian (with variance $\gamma^2 = 1$) and b) a Cauchy spin distribution (with scale parameter $\gamma = 1$). Again a splitting is observed as well as a linear behaviour below T_{fs} (T_{fs} depends on the distribution used).

All of the distributions show a linear behaviour of σ_L^2 below an onset temperature T_{fs} and a splitting for different system sizes. The exact value for T_{fs} depends on the distribution used but the qualitative behaviour is the same for all distributions. The variances of the underlying distributions rescales the temperature e.g. $T' \propto \gamma T$ (for the gamma distribution) and could have been adjusted to make the comparison more clear.

To get further insight into the low temperature behaviour of such models we used the 2d fast fourier transform (FFT) of the correlation function (with subtracted instantaneous spatial average) to extract the scaling exponent μ for the correlation length. For an arbitrary spin distribution this correlation function with respect to a reference spin $s_{0,0}$ can be expressed as (see section 6.3.3 for details):

$$G(s_{0,0}, s_{0+d,0+e}) := G_{de} = \sum_{n,m=0}^{L-1}{}' \left\langle a_{nm}^2 \cos(\frac{2\pi n}{L} d) \cos(\frac{2\pi m}{L} e) \right\rangle_t$$

Figure 45 shows a log-log plot of the mode amplitude $|a_{nm}|^2$ versus $k := |\vec{k}|$, with $\vec{k} = (n, m)^\perp$. This was done for uniform distributions and $L = 32$ only.

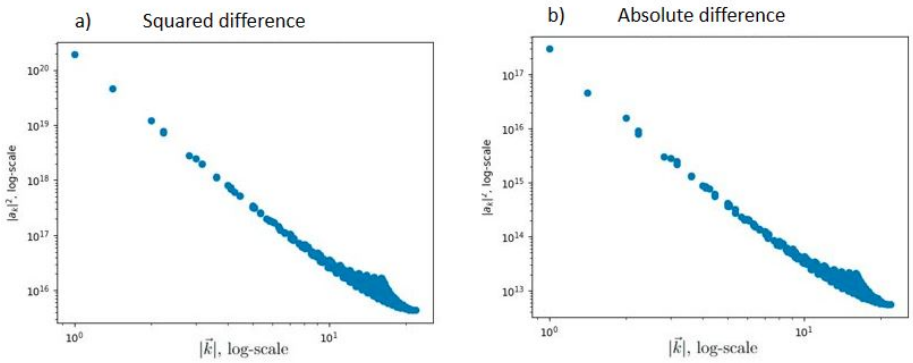

Figure 45: Mode amplitude plotted against $|\vec{k}|$ for a $L = 32$ system. Example for a) squared difference and b) absolute difference interactions and an underlying Gaussian distribution to generate the spins. The departure from the linear behaviour is caused by the cosine terms which contribute for large $|\vec{k}|$.

Changing the interactions left the slope of the linear curve unchanged. From the slope we can read of the behaviour of the fourier amplitudes $|a_k|^2 \propto |\vec{k}|^{-2}$. This corresponds to a mean field exponent $[\eta = \eta_{MF} = 0]$ as shown by Ornstein and Zernike (see section 6.3.3 and appendix for details) [60].

6.3 Analytical model

The above considerations show that gradient models with continuous spin distribution below T_{fs} behave all similar to the 2d N-state Ising model. Therefor we will look at a Gaussian-like model which is analytically solvable. We will introduce the Gaussian Hamiltonian and solve it. We are then able to calculate σ_L^2 explicitly which enables us to get insight into the apparent scaling law we saw in section 5. For simplicity we use scalar spins but it is straight forward to generalise the results to higher spin dimensions.

6.3.1 The Gaussian Model

The Hamiltonian of the model in the semi-grand canonical ensemble is given by squared-difference interactions and an entropic external field like term with underlying Gaussian density of states:

$$\mathcal{H}_{G'} = J \sum_{\langle i,j \rangle} (s_i - s_j)^2 - k_B T \sum_i \ln\left(\Omega(s_i)\right) = \mathcal{H}_{G'_1} + \mathcal{H}_{G'_2}$$

where $J > 0$, the sum runs over nearest neighbours and $\Omega(s_i) = \gamma^{-1} \exp\left(-\frac{s_i^2}{2\gamma^2}\right)$ is the continuous density of states with underlying Gaussian distribution and variance γ. The Gaussian is centered around 0 and we set $\gamma = 1$ (the exact value rescales the temperature again $T' \propto \gamma^2 T$). For later convenience we split the Hamiltonian into two parts: $\mathcal{H}_{G'_1}$ is the interaction part and $\mathcal{H}_{G'_2}$ the entropic external field part. If we write out the nearest neighbour interactions explicitly we get:

$$\mathcal{H}_{G'} = J \sum_{i,j=0}^{L-1} \left(\left[s_{i,j} - s_{i+1,j}\right]^2 + \left[s_{i,j} - s_{i,j+1}\right]^2 \right) - k_B T \sum_{i,j=0}^{L-1} \ln\left(\Omega(s_{i,j})\right)$$

$$= 2J \sum_{i,j=0}^{L-1} s_{i,j}^2 \left(2 - s_{i,j}\left(s_{i+1,j} + s_{i,j+1}\right)\right) + \frac{1}{2} k_B T \sum_{i,j=0}^{L-1} s_{i,j}^2$$

where $\sum_{i,j=0}^{L-1} s_{i+1,j}^2 = \sum_{i,j=0}^{L-1} s_{i,j}^2$ for periodic boundary conditions was used and the sum over nearest neighbours only is written out for two of the four neighbours in order to avoid double counting.

Since we only have square terms for the spins the Hamiltonian decouples in fourier space. The spins are real and we use a cosine expansion instead of complex exponentials. We will use the basis $s_{i,j} = \frac{2}{L} \sum_{n,m=0}^{L-1} a_{nm} \cos(\frac{2\pi n}{L} i) \cos(\frac{2\pi m}{L} j)$, where n and m are the fourier indices and a_{nm} is the fourier coefficient of mode $\{n, m\}$. Then the transform of the sum over the squared spins is:

$$\sum_{i,j=0}^{L-1} s_{i,j}^2$$

$$= \frac{4}{L^2} \sum_{i,j=0}^{L-1} \sum_{n,m=0}^{L-1} \sum_{n',m'=0}^{L-1} a_{nm} a_{n'm'} \cos\left(\frac{2\pi n}{L} i\right) \cos\left(\frac{2\pi m}{L} j\right) \cos\left(\frac{2\pi n'}{L} i\right) \cos\left(\frac{2\pi m'}{L} j\right)$$

Performing the sum over $\{i, j\}$ yields 0 if $\{n', m'\} \neq \{n, m\}$, therefor we get Parseval's theorem:

$$\sum_{i,j=0}^{L-1} s_{ij}^2 = \frac{4}{L^2} \sum_{n,m=0}^{L-1} \sum_{i,j=0}^{L-1} a_{nm}^2 \cos^2\left(\frac{2\pi n}{L} j\right) \cos^2\left(\frac{2\pi m}{L} l\right) = \sum_{n,m=0}^{L-1} a_{nm}^2$$

Where $\sum_{i=0}^{L-1} \cos^2(\frac{2\pi n}{L} i) = L/2$ was used for the last equality. The other terms in $\mathcal{H}_{G_1'}$ yield:

$$\sum_{i,j=0}^{L-1} s_{i,j} s_{i+1,j} = \frac{4}{L^2} \sum_{n,m=0}^{L-1} \sum_{i,j=0}^{L-1} a_{nm}^2 \cos\frac{2\pi n}{L} i \ \cos(\frac{2\pi n}{L}(i+1)) \cos^2(\frac{2\pi m}{L} j)$$

$$= \sum_{n,m=0}^{L-1} a_{nm}^2 \cos(\frac{2\pi n}{L})$$

where $\sum_{i=0}^{L-1} \cos(\frac{2\pi n}{L} i) \cos(\frac{2\pi n}{L}(i+1)) = \frac{L}{2} \cos(\frac{2\pi n}{L})$ was used.
With that the Hamiltonian becomes

$$\mathcal{H}_{G'} = \sum_{n,m=0}^{L-1} a_{nm}^2 \left(\frac{1}{2} k_B T + 2J \left(2 - \left[\cos(\frac{2\pi n}{L}) + \cos(\frac{2\pi m}{L})\right]\right)\right)$$

Lets define $b_{nm} = 2 - [\cos(\frac{2\pi n}{L}) + \cos(\frac{2\pi m}{L})]$.
Now we can write down the partition function with a (convenient) normalization constant:

$$Z(\beta) = \frac{1}{\sqrt{2\pi}} \prod_{n,m=0}^{L-1} \int_{-\infty}^{\infty} da_{nm} \exp\left(-\beta a_{nm}^2 \left[\frac{1}{2} k_B T + 2J b_{nm}\right]\right)$$

The above is a Gaussian integral $\int_{-\infty}^{\infty} dx e^{-a(x+b)^2} = \sqrt{\frac{\pi}{a}}$ such that:

$$Z(\beta) = \frac{1}{\sqrt{2\pi}} \prod_{n,m=0}^{L-1} \sqrt{2\pi / [\beta(k_B T + 4J b_{n,m})]} = \exp\left(\sum_{n,m=0}^{L-1} \ln[(1 + 4J\beta b_{n,m})]^{-0.5}\right)$$

$$= \exp\left(-\sum_{n,m=0}^{L-1} \ln\sqrt{1 + 4J\beta b_{nm}}\right)$$

Unfortunately it is not possible to analytically solve the sum over b_{nm} due to the cosine terms. But still we can now in principle derive all observables from the partition function. Approximations we make can be checked easily since the computer has no trouble computing the exact sum even for large values of L. Furthermore we will check our analytical results against simulations.

6.3.2 Observables of the Gaussian model

We start with **thermal average of the fourier coefficients**. Since the modes decouple in fourier space we can read of $< a_{nm}^2 >= k_B T/\kappa$ (equipartition theorem) which immediately gives:

$$< a_{nm}^2 >= k_B T/(k_B T + 4Jb_{nm})$$

Also the **free energy** is straightforward to write down:

$$F = -k_B T \ln(Z) = k_B T \sum_{n,m} \ln \sqrt{1 + 4\beta J b_{nm}}$$

Energy moments

For the computation of the internal energy and heat capacity the code uses only the interaction term $\mathcal{H}_{G_1'}$ of the model. Analytically we can achieve this for example by assigning two different 'inverse temperature parameters' (β_1, β_2) to the partition function:

$$Z(\beta_1, \beta_2) = \frac{1}{\sqrt{2\pi}} \prod_{n,m=0}^{L-1} \int_{-\infty}^{\infty} da_{nm} \exp\left(-a_{nm}^2 \left[2J\beta_1 b_{nm} + \frac{1}{2} k_B T \beta_2 \right] \right)$$

$$= \exp\left(- \sum_{n,m=0}^{L-1} \ln \sqrt{k_B T \beta_2 + 4J\beta_1 b_{nm}} \right)$$

The **internal energy** is then:

$$< E >= -\frac{\partial \ln(Z(\beta_1, \beta_2))}{\partial \beta_1} = \sum_{n,m} \frac{Jb_{nm}}{2J\beta_1 b_{nm} + k_B T \beta_2} = 2J \sum_{n,m} b_{nm} [1 + 4\beta J b_{nm}]^{-1}$$

where in the last step we then set $\beta_1 = \beta_2 = \beta$.

From the mean energy we can obtain the **heat capacity** at constant volume C_V:

$$C_V = -\frac{1}{k_B T^2} \frac{\partial}{\partial \beta_1} < E >= \frac{8J^2}{k_B T^2} \sum_{n,m} b_{nm}^2 [k_B T \beta_2 + 4\beta_1 J b_{nm}]^{-2}$$

$$= \frac{8J^2}{k_B T^2} \sum_{n,m} b_{nm}^2 [1 + 4\beta J b_{nm}]^{-2}$$

Figure 46 shows the right trend for the intrinsic heat capacity.

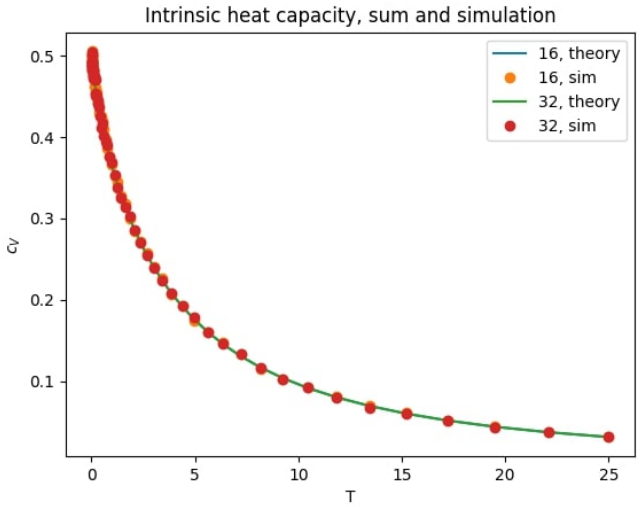

Figure 46: Comparison of intrinsic heat capacities for the analytic result and simulation for 2 system sizes.

The Variance(s) of spins:

There are 2 variances computed by the code which used to characterise the spin distributions below T_{fs} (see section 5). The first one is the usual **spin variance**:

$$\sigma^2 = \langle s_{i,j}^2 \rangle - \langle s_{i,j} \rangle^2$$

The 2nd term is 0 because we draw the spins from a Gaussian distribution centered around 0. The first term is straight-forward using our earlier result

$$\langle s_{i,j}^2 \rangle = \sum_{n,m=0}^{L-1} \langle a_{nm}^2 \rangle_t$$

Here we used that we can rewrite the thermal average $\langle . \rangle_{th}$ as $\langle \langle . \rangle_L \rangle_t$ where $\langle . \rangle_L$ again is the instantaneous lattice average. So (see figure 47):

$$\sigma^2 = \sum_{n,m=0}^{L-1} \langle a_{nm}^2 \rangle_t$$

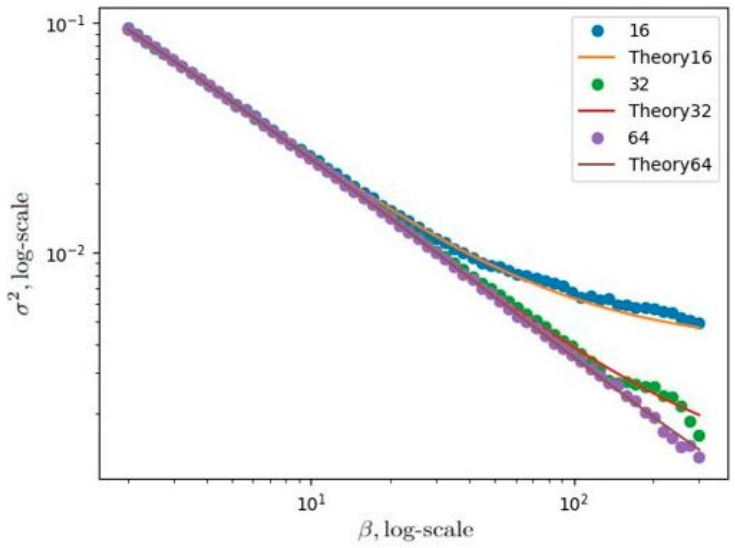

Figure 47: Spin variance σ^2 theory against simulation for 3 system sizes (label).

The other variance term computed by the code is the **'spatial'** or **instantaneous spin variance** where the instantaneous lattice average is subtracted from the random spin variable:

$$\sigma_L^2 = \left\langle (s_{i,j} - \langle s_{i,j} \rangle_L)^2 \right\rangle - \left\langle s_{i,j} - \langle s_{i,j} \rangle_L \right\rangle^2$$

The instantaneous lattice average is just the $\{0,0\}$-th mode in fourier space:

$$\langle s_{i,j} \rangle_L = \frac{1}{L^2} \sum_{i,j=0}^{L-1} s_{i,j} = \frac{1}{L^2} \frac{2}{L} \sum_{i,j=0}^{L-1} \sum_{n,m=0}^{L-1} a_{nm} \cos(\frac{2\pi n}{L} i) \cos(\frac{2\pi m}{L} j)$$

If $\{n,m\} \neq \{0,0\}$ the sum over space becomes 0 due to the cosine terms. If $\{n,m\} = \{0,0\}$ the cosine terms are 1 and the sum over space just gives L^2. Therefor:

$$\langle s_{i,j} \rangle_L = \frac{2}{L} a_{00}$$

The second term of σ_L^2 equals 0:

$$\left\langle s_{i,j} - \langle s_{i,j} \rangle_L \right\rangle_{th} = \left\langle \frac{2}{L} \sum_{i,j=0}^{L-1} \left(\sum_{n,m=0}^{L-1} a_{nm} \cos(\frac{2\pi n}{L} i) \cos(\frac{2\pi m}{L} j) - \frac{2}{L} a_{00} \right) \right\rangle_t$$

$$\left\langle \frac{2}{L} \sum_{i,j=0}^{L-1} \left({\sum_{n,m=0}^{L-1}}' a_{nm} \cos(\frac{2\pi n}{L} i) \cos(\frac{2\pi m}{L} j) \right) \right\rangle_t = 0$$

since $\{n, m\}$ cannot be $\{0, 0\}$ now. $\sum'$ indicates that the $\{0, 0\}$ mode is omitted.

The first term is therefor just σ^2 without the $\{0, 0\}$-mode:

$$\left\langle (s_{0,0} - \langle s_{i,j} \rangle_L)^2 \right\rangle = \left\langle \frac{2}{L} \sum_{n,m=0}^{L-1} \sum_{i,j=0}^{L-1} a_{nm} \cos(\frac{2\pi n}{L} i) \cos(\frac{2\pi m}{L} j) - \frac{2}{L} a_{00} \right)^2 \Bigg\rangle_t$$

$$= {\sum_{n,m=0}^{L-1}}' \left\langle a_{nm}^2 \right\rangle_t$$

So explicitly (see figure 48):

$$\sigma_L^2 = {\sum_{n,m=0}^{L-1}}' \left\langle a_{nm}^2 \right\rangle_t$$

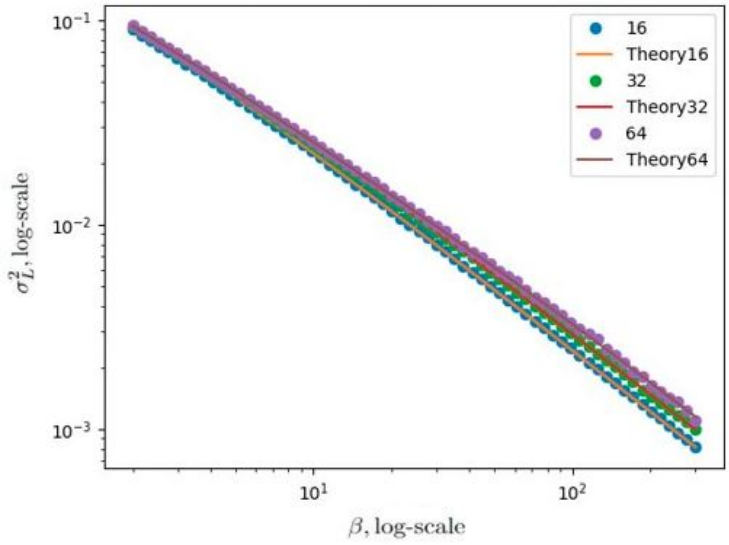

Figure 48: Instantaneous spin variance σ_L^2 theory against simulation for 3 system sizes (label).

The Correlation Function

The correlation function is given by the covariance of two spins separated by a distance $\{d, e\}$. The instantaneous lattice average is again subtracted from the random spin variable and we omit the second term which is given by $\left\langle s_{i,j} - \langle s_{i,j}\rangle_L \right\rangle_{th} \left\langle s_{i+d,j+e} - \langle s_{i,j}\rangle_L \right\rangle_{th}$ because it equals 0 again (as for σ_L^2).

$$G(s_{i,j}, s_{(i+d)(j+e)}) = \left\langle (s_{i,j} - \langle s_{i,j}\rangle_L)(s_{i+d,j+e} - \langle s_{i,j}\rangle_L \right\rangle$$

Without loss of generality we choose $s_{0,0}$ as a reference spin. Using the result from σ_L^2 we can simplify:

$$G(s_{0,0}, s_{0+d,0+e}) := G_{de}$$

$$= \frac{4}{L^2} \left\langle \sum_{i,j=0}^{L-1} \sum_{n,m=0}^{L-1}{}' a_{nm} \sum_{n',m'=0}^{L-1}{}' a_{n'm'} \cos(\frac{2\pi n'}{L} d) \cos(\frac{2\pi m'}{L} e) \right\rangle_t$$

$$= 4 \sum_{n,m=0}^{L-1}{}' \left\langle a_{nm}^2 \cos(\frac{2\pi n}{L} d) \cos(\frac{2\pi m}{L} e) \right\rangle_t$$

When $\{d, e\} = \{0, 0\}$ we want $G_{de} = 1$ (normalized). Therefor we have to divide by the distributions instantaneous variance:

$$G_{de} = \sum_{n,m=0}^{L-1}{}' \left\langle a_{nm}^2 \cos(\frac{2\pi n}{L} d) \cos(\frac{2\pi m}{L} e) \right\rangle_t / (\sum_{n,m=0}^{L-1}{}' \left\langle a_{nm}^2 \right\rangle_t)$$

To check the theory against the simulation we plot G_{de} in one spatial direction e.g. by setting $e = 0$ (see figure 49).

Magnetization

The magnetization is equal 0 for all $T > 0$ since our Hamiltonian is quadratic and the Gaussian spin-distribution is centered around 0. This model does not have a phase transition for any $T > 0$.

$$\langle m \rangle = \frac{1}{L^2} \sum_{i,j=0}^{L^2-1} s_{i,j} = \frac{1}{L^2} \sum_{i,j=0}^{L^2-1} \sum_{n,m=0}^{L^2-1} a_{nm} \cos\left(\frac{2\pi n}{L} i\right) \cos\left(\frac{2\pi m}{L} j\right)$$

which is equal 0 since the sums can be interchanged and $\sum_{i=0}^{L^2-1} \cos\left(\frac{2\pi n}{L} i\right) = 0$.

6.3.3 Mean field exponents

Now we want to verify that this model belongs to the mean field universality class. Therefor we calculate two exponents of the model for infinite size in the limit $T \longrightarrow 0$.

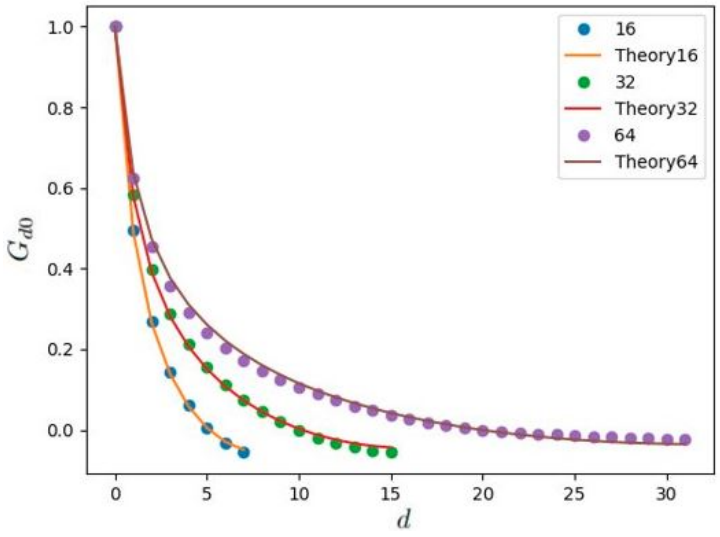

Figure 49: Theory vs simulation of the correlation function for 3 system sizes (label) for low temperatures. Due to the periodic boundary conditions only half of the grid length is uncorrelated.

We start with the exponent for the correlation function where it is sufficient to use the unnormalized quantity. We can exploit the summation over cosines again if we transform the correlation function to fourier space:

$$\mathcal{F}(G_{de}) = \frac{2}{L}\sum_{d,e=0}^{L-1}\sum_{n,m=0}^{L-1}{}' \left\langle a_{nm}^2 \cos(\frac{2\pi n}{L}d)\cos(\frac{2\pi m}{L}e)\cos(\frac{2\pi n'}{L}d)\cos(\frac{2\pi m'}{L}e)\right\rangle_t$$

$$= \sum_{n,m=0}^{L-1}{}' \left\langle a_{nm}^2\right\rangle_t$$

To explore the behaviour in the thermodynamic limit we take the limit $L \longrightarrow \infty$. For large L one can approximate the sum as an integral since the modes lie close together. Furthermore we approximate $1-\cos(\frac{2\pi n}{L}) \approx \frac{2\pi^2 n^2}{L^2}$ (this is rationalized in section 6.6) and perform our calculation in the first Brioullin zone. We obtain an *Ornstein-Zernike* form:

$$\mathcal{F}(G_{de}) \approx \int_{-L/2}^{L/2}\int_{-L/2}^{L/2}\frac{1}{1+\frac{8J\pi^2}{k_BTL^2}(n^2+m^2)}dndm - \int_{-\epsilon}^{\epsilon}\int_{-\epsilon}^{\epsilon}\left\langle a_{nm}^2\right\rangle_t dndm$$

where the subtraction stems from the $\{0,0\}$-mode. The fourier amplitude for $\{n,m\}=\{0,0\}$ is finite and we can treat the subtraction as small. The Ornstein-

Zernike form is given by:

$$\mathcal{F}(G_{OZ}) \propto \int_{|\vec{k}|} \frac{1}{1+\xi^2(T)|\vec{k}|^2} d|\vec{k}|$$

If one transforms $\mathcal{F}(G_{OZ})$ back to real space we get $G(r) \propto 1/r^{d-2+\eta}$ where $\eta = 0 = \eta_{MF}$ for $|\vec{k}|^2$ in the integral (see Appendix). Thus confirming the first mean field exponent.

Additionally we obtain an approximate form for the correlation length, which depends on T and L:

$$\xi(T) \approx \sqrt{\frac{8J\pi^2}{k_B T L^2}}$$

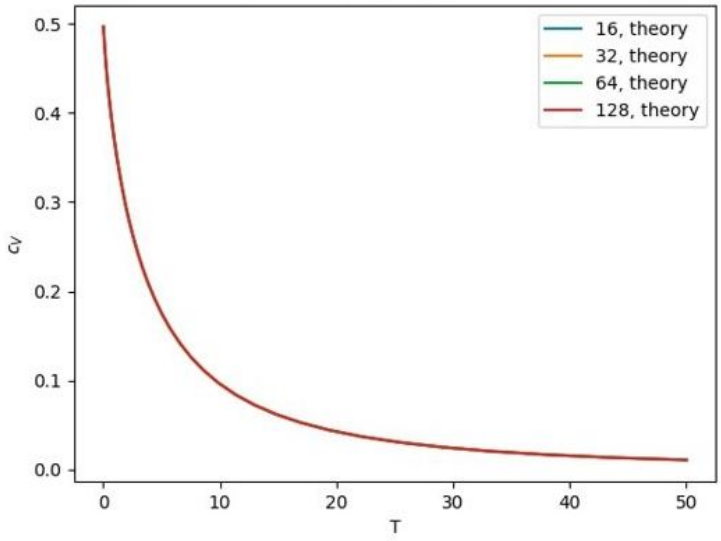

Figure 50: Intrinsic heat capacity c_V for 4 different system sizes (label) computed from the analytical results (sum).

The second exponent was obtained from the analytical expression of the heat capacity which takes on a constant value of $1/2$ as $T \longrightarrow 0$ independent of system size (see figure 50). Since their is no divergence as $T_c = 0$ is approached we know $\alpha = 0$ which again is a mean field exponent.

6.3.4 Looking for the apparent scaling exponent

In section 5 the apparent exponent was found in the instantaneous spin variance σ_L^2. Below T_{fs} it becomes linear ($\sigma_L^2 \propto T$) and deviates from the ensemble averaged spin variance σ^2. The ratio of σ_L^2 for different system sizes was found

to be a constant value of 1/5. We find a similar behaviour for our model here (see figure 51). But for the Gaussian model the variance σ^2 settles on a system size depending value.

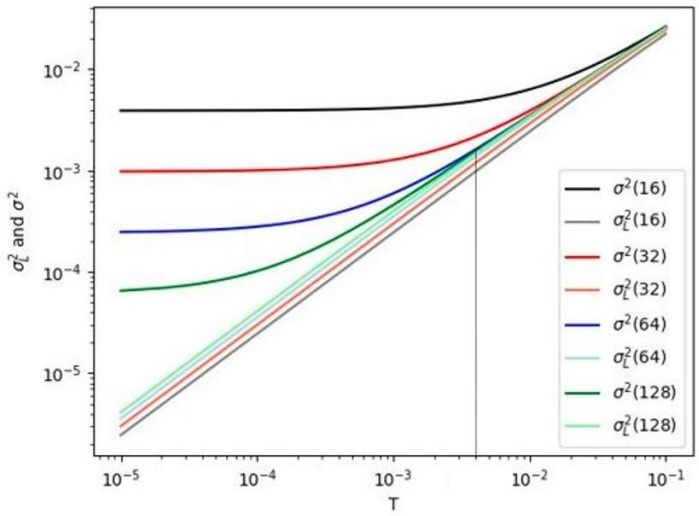

Figure 51: Variance σ^2 and instantaneous variance σ_L^2 for the Gaussian model. Again we find distinct behaviour of the quantities below an system size depending onset temperature (here only visually indicated by the black line). σ^2 settles at a value $1/L^2$ and for $L \longrightarrow \infty$ the quantities seem to become identical. The label indicates the system sizes.

To explore the apparent scaling law we take the analytical result for σ_L^2 and explore the limiting case as $T \longrightarrow 0$ and $L \longrightarrow \infty$. The order to take the limits is important and it is not clear in which order to take them.

General case first:

First we will look at the case where we take the general equation for σ_L^2 and send $L \longrightarrow \infty$. Let's write down the expression for σ_L^2 again:

$$\sigma_L^2 = \sum_{n,m=0}^{L-1}{}' \left\langle a_{nm}^2 \right\rangle_t = \sum_{n,m=0}^{L-1}{}' \frac{k_B T}{k_B T + 4J b_{n,m}}$$

where again $b_{nm} = 2 - [\cos(\frac{2\pi n}{L}) + \cos(\frac{2\pi m}{L})]$. Since all 4 quarters of the first Brioullin zone contribute equally we only look at 1 quarter and multiply by 4. For L large enough we can replace the sum by an integral but we have to be careful to include all the parts (since we cut out a square at the origin for σ_L^2).

The cut-out parts have equal portions and we get:

$$\sigma_L^2 \approx \frac{4}{L^2}\left[\int_1^{L/2} dn \int_1^{L/2} dm \frac{1}{1+\frac{4J}{k_BT}b_{nm}} + 2\int_1^{L/2} dn \int_0^{1} dm \frac{1}{1+\frac{4J}{k_BT}b_{nm}}\right]$$

We then use the substitution $x = n/L$ and $y = m/L$ (see figure 52) and b_{nm} becomes $b_{xy} = 2 - \cos(2\pi x) - \cos(2\pi y)$. This highlights the contribution of the origin with system size which is approached as $1/L$. This contribution is the difference between σ^2 and σ_L^2. We get:

$$\sigma_L^2 = 4\left[\int_{1/L}^{1/2} dx \int_{1/L}^{1/2} dy \frac{1}{1+\frac{4J}{k_BT}b_{xy}} + 2\int_{1/L}^{1/2} dx \int_0^{1/L} dy \frac{1}{1+\frac{4J}{k_BT}b_{xy}}\right]$$

To be able to solve the integral we again approximate $\cos(2\pi x) \approx 1 - 2\pi^2 x^2$. This valid for small $\{n, m\}$ and these modes should contribute the most at low temperatures as L increases (see small temperature expansion (next part)). In figure 52 the slightly shaded area is what is left out by the integral for σ_L^2 whereas the integral for σ^2 leaves out no mode. The integral becomes:

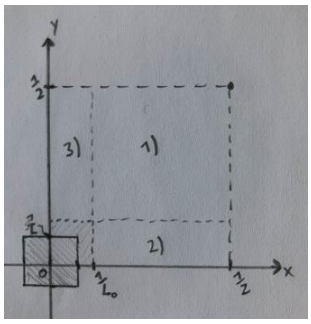

Figure 52: Sketch of the integral calculation for substituted variables x and y.

$$\sigma_L^2 \approx 4\left[\int_{1/L}^{1/2} dx \int_{1/L}^{1/2} dy \frac{1}{1+\frac{4J}{k_BT}(x^2+y^2)}\right.$$

$$\left. +2\int_{1/L}^{1/2} dx \int_0^{1/L} dy \frac{1}{1+\frac{4J}{k_BT}(x^2+y^2)}\right]$$

$$= 4\int_{1/L}^{1/2} dr \int_0^{\pi/2} d\varphi \frac{r}{1+\frac{4J}{k_BT}r^2} = 2\pi \ln\left[\frac{1+\frac{2\pi^2 J}{k_BT}}{1+\frac{8\pi^2 J}{k_BTL^2}}\right]$$

Thus we see that this limit only tells us that σ_L^2 does not diverge as L is increased at any finite temperature.

Small temperature expansion:

In the limit $T \longrightarrow 0$ we can replace the term in the sum by a geometric series (series expansion around $T = 0$):

$$\frac{kT}{kT + 4Jb_{nm}} = \frac{kT}{4Jb_{nm}} - \mathcal{O}(T^2)$$

Since we saw a linear behaviour below T_{fs} is it sufficient to expand the series only up to first order. Now we see that σ^2, which includes the $\{0, 0\}$-mode diverges

in this low T expansion. Since σ_L^2 approaches σ^2 for $L \longrightarrow \infty$ the modes close to the origin should contribute the most, justifying the cosine expansion.

We can make the same simplifications as before and end up with a polar integral. With that we obtain our final result:

$$\sigma_L^2 \approx \frac{k_B T}{2\pi^2 J} \int_{1/L}^{1/2} dr \int_0^{\pi/2} d\phi \frac{1}{r} = \frac{k_B T}{4\pi J} \ln(L/2)$$

This logarithmic divergence is confirmed by comparing it to the sum expression for the series expansion around $T = 0$. At large values of L the curves are in good agreement (see figure 53).

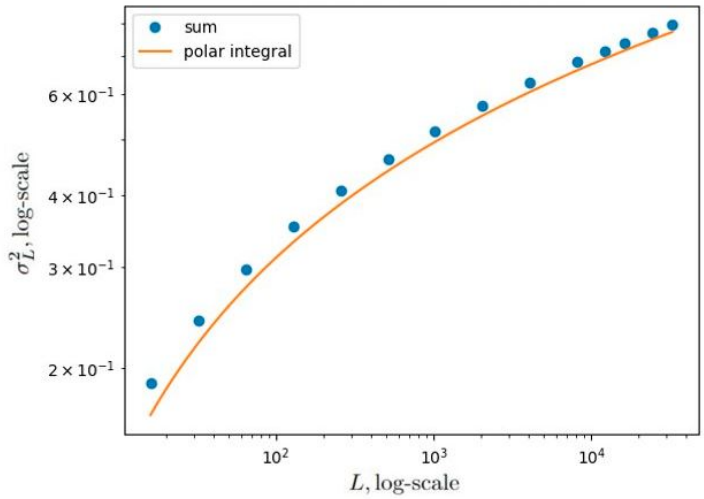

Figure 53: Confirmation of the logarithmic divergence of σ_L^2 with system size in the linear (low T) regime.

In this model the apparent 0.2 exponent turns out to be a logarithmic behaviour with system size for finite sizes. But note if L is large the linear T expansion is not valid anymore since σ_L^2 never diverges.

6.3.5 Independence of order parameter dimension

Lastly I quickly want to mention the independence of the order parameter dimension in the Gaussian model. Recall the Hamiltonian for the scalar spins:

$$\mathcal{H}_{G'} = 2J \sum_{i,j=0}^{L-1} s_{i,j}^2 \left(2 - s_{i,j} \left(s_{i+1,j} + s_{i,j+1}\right)\right) + \frac{1}{2} k_B T \sum_{i,j=0}^{L-1} s_{i,j}^2$$

It only has contributions where the spins appear squared. Therefor it decoupled in Fourier space:

$$\mathcal{H}_{G'} = \sum_{n,m=0}^{L-1} a_{nm}^2 \left(\frac{1}{2} k_B T + 2J b_{nm} \right)$$

with $b_{nm} = 2 - [\cos(\frac{2\pi n}{L}) + \cos(\frac{2\pi m}{L})]$. If we use vector spins in the Hamiltonian we get terms like $\vec{s}^2$ in it. These themselves can be written as a sum $\vec{s}^2 = \sum_{i=1}^{d} s_i^2$ where d is the spin dimension. Therefor the modes of a cosine expansion again decouple and each spin dimension contributes identically:

$$\mathcal{H}_{G'} = \sum_{i=1}^{d} \left(\sum_{n,m} a_{nm}^2 \left(\frac{k_B T}{2} + 2J b_{nm} \right) \right)_i$$

This again motivates to rigorously test if the results for models similar to the 2d N-state Ising model are independent of the order parameter dimension.

7 Summary and Outlook

In this work we have explored the peculiar behaviour of the 2d N-state Ising Hamiltonian further. From simulations we saw that finite size effects like the critical plateau region for the correlation length, persisting over a range of temperatures, is independent of the order parameter dimension. Systems which were equilibrated deep in the plateau regime below an onset temperature T_{fs} show demixing when the systems instantaneous variance is constrained. These results seem to be robust under the exact form of the Hamiltonian. Furthermore we saw that we can approximate the various Hamiltonians by an analytically solvable Gaussian model below T_{fs}. Here we again found a difference between temporal and spatial averages ($\sigma^2 \neq \sigma_L^2$) and the apparent scaling law in this model is a logarithmic effect which vanishes for big system sizes.

The extension of the order parameter dimension could be used to expand the chemical space by e.g. including head group interactions of lipids as well, since it introduces another degree of freedom to the system. Thus making the model robust to even more complicated systems, naturally explaining how a complicated cell membrane could organise itself without the need to tune its composition explicitly. However it is not clear if proteins can be included straight forwardly since they often posses specific lipid binding domains ('fingerprints') [61].

Our model predicts that cells would adapt their lipid composition (in our model $\sigma_L^2 \propto T$ below T_{fs}) to always remain close to a critical demixing transition. An ongoing debate about cell membranes is whether they posses some lateral organization and homogeneities which are termed lipid rafts [62]. These are regions of liquid ordered domains where specific lipids and proteins are concentrated to provide platforms which e.g. could facilitate reactions with membrane proteins and the environment. In our model the enhanced correlation lengths suggest that lipid rafts could arise from critical behaviour. However, for micron-sized ($\sim$ cell size) systems ($L \approx 64 - 256$) the correlation lengths are too big, since rafts are predicted to be only of size $10 - 200nm$. A possible 'natural limitation' for the correlation lengths could arise through the cytoskeleton. It is a dynamic network of actin filaments extending through the cytoplasm as well as across the inner leaflet of the plasma membrane. A network runs along the inner leaflet and they form a rather long lived bond where they are anchored in the plasma membrane. There they restrict the lateral diffusion of the membrane components by creating fixed points in the membrane. This disrupts the long correlations to the typical cytoskeleton-network size of $40 - 230nm$ [48].

Also chemostatic controlled components could cause a similar effect. Cholesterol for example has ideal fractions for which the membrane functions optimally but it gets constantly removed or added to it [63]. In an environment which constantly changes the cell adapts a steady state of cholesterol levels to keep their levels constant. Cholesterol is associated with liquid ordered raft domains: they control membrane fluidity and raft domains are thought to be more solid like [2]. Proteins with specific lipid binding domains could further enhance phase separation and domain formation and it would be interesting to try to include

them in our model.

It is still not clear how to theoretically model the GPMV experimental procedure. Thermodynamic systems should be describable in any ensemble since they are all connected by Legendre transformations. But below T_{fs} we observe demixing in our model when we constrain the spins which does not occur in the unconstrained system. This seems to be stemming from non-ergodic behaviour in that regime for finite systems. But this behaviour vanishes for $L \longrightarrow \infty$ and it is unclear how to e.g. properly extract critical exponents since we do not have a true fixed point.

Although we did not find the apparent scaling law in the analytical model it is still unclear whether it translates to the 2d N-state Ising model. It has an underlying uniform distribution which has highly correlated fourier modes while a Gaussian model has completely decoupled fourier modes. The uniform distribution can be parameterised as $\Omega(s) \propto \exp(-|s|^m)$ for $m \longrightarrow \infty$ and even. The scaling could stem from cross-correlations where one must include higher order spin contributions to the chemical potential, for example as pertubative effects to the Gaussian model. This is reminiscent of a Φ^4-theory where a quartic term introduces 'interactions' to a free field theory.

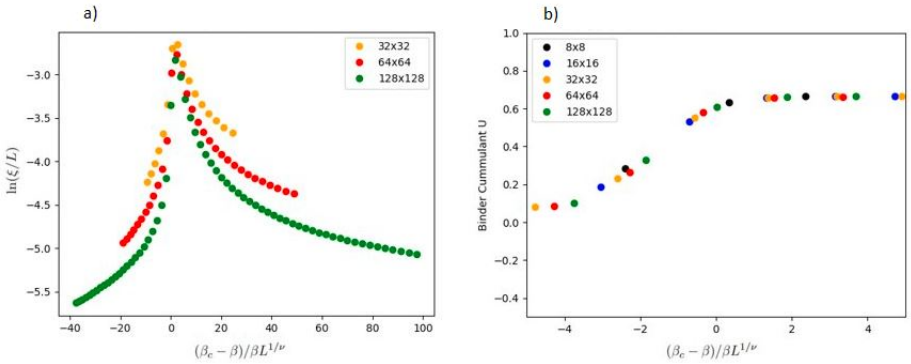

Figure 54: Rescaled a) correlation length and b) Binder cumulant as a function of the reduced inverse temperature. The correlation length peak collapses in the vicinity to the critical reduced inverse temperature with $(T - T_c)/T_c = (\beta_c - \beta)/\beta$. $\xi \propto L$ at the critical point and the Binder cumulant is given by $U = 1 - \langle s^4 \rangle / (3 \langle s^2 \rangle^2)$.

A Appendix

A.1 Ising Model

First the code was tested by verifying the known scaling laws of the 2D Ising model. The model was implemented with $s = 0.5, 1$ and absolute differences which lead to $T_c' = T_c/4$. The collapsed plots verify T_c'.

Susceptibility:
The finite size scaling (FSS) is derived as follows: Since $\xi \propto t^{-\nu}$ and $\xi \propto L$ near $T = T_c$ with $t = (T - T_c)/T_c$ we can rewrite $\chi \propto t^{-\gamma} = \xi^{\nu/\gamma} = L^{\nu/\gamma}$. For the x-axis we can directly use $t \propto \xi^{\nu} = L^{\nu}$. To collapse the curves we have to rescale the plots with the inverse exponents. $\nu = 1$ and $\gamma = 7/4$ for the 2D Ising model.

Binder cumulant
It collapses by construction for rescaled x-axis.

Correlation Length
Here also the y-axis is rescaled as ξ/L since $\nu = 1$. For more accuracy at T_c the log was taken as well.

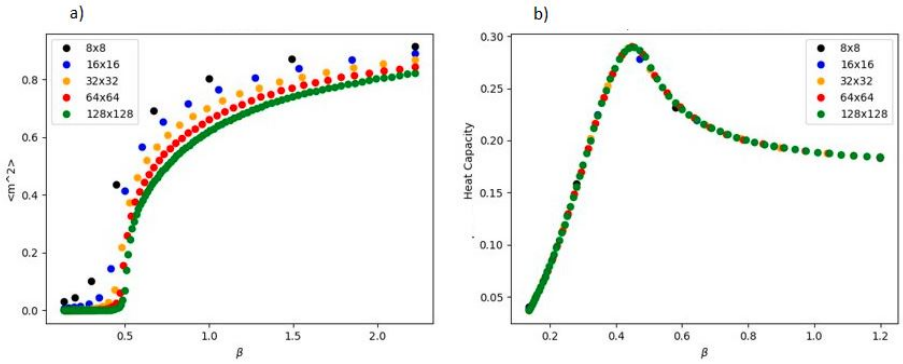

Figure 55: Testing the code with the XY model. a) Mean square magnetization $< m^2 >$ against inverse temperature β. Again $\beta'_{BKT} \approx 0.565$ is verified visually. For the calculation for β'_{BKT} see (section 6.1.1) b) Heat capacity, showing a feature below T_{BKT}. It is independent of system size which and consistent with results of Nguyen [64].

A.2 XY Model

A.2.1 XY model correlations

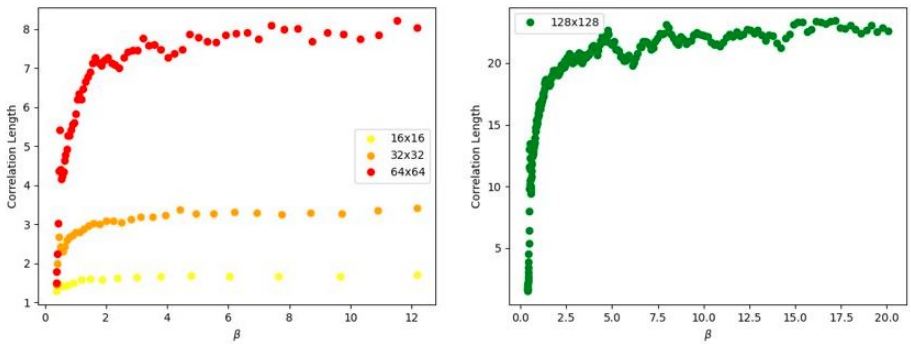

Figure 56: Correlation length over a **wider range** of inverse temperatures β for the 2D XY model, crossing β_{BKT}.

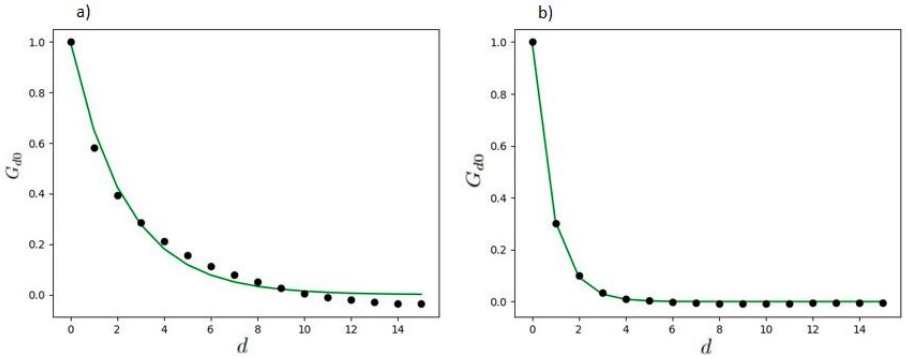

Figure 57: Correlation function in one spatial direction d fitted by an exponential $\exp(-d/\xi)$ where ξ is the correlation length for $L = 32$. For T a) below T_{fs} and b) far above T_{fs}.

A.2.2 XY model patching and demixing

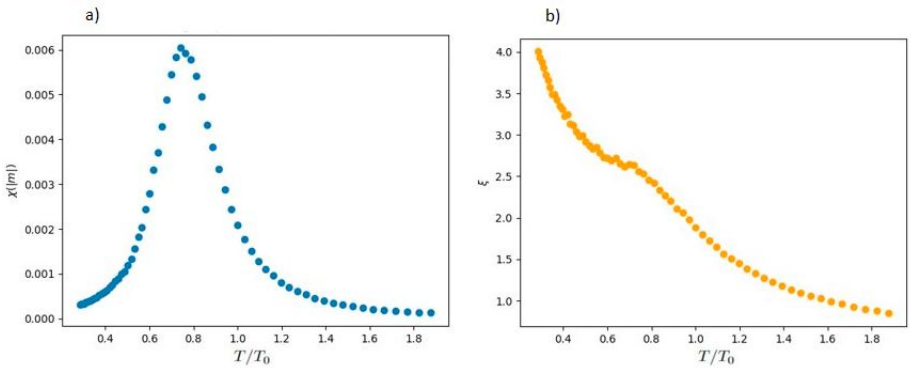

Figure 58: a) Susceptibility and b) correlation length show a small peak at the same T/T_0 value which is identified with the demixing temperature T_{demix}.

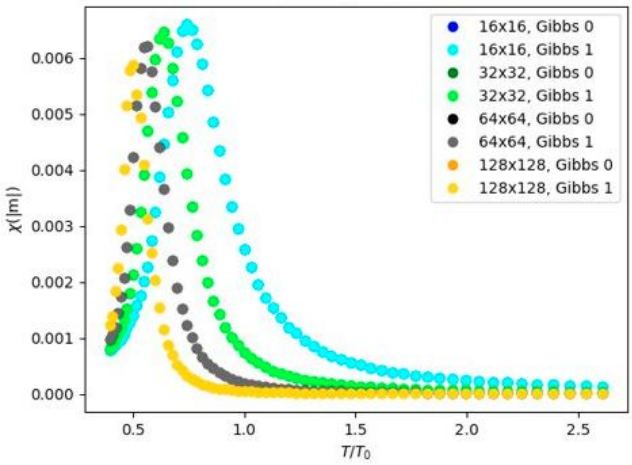

Figure 59: An example of unrescaled susceptibilities of the freezing and patching procedure (see section 6.1.2). Visually $T_{\text{demix}} \longrightarrow 0$ as $L \longrightarrow \infty$. The symmetry of the Gibbs frames for observables regarding $|m|$ is visible.

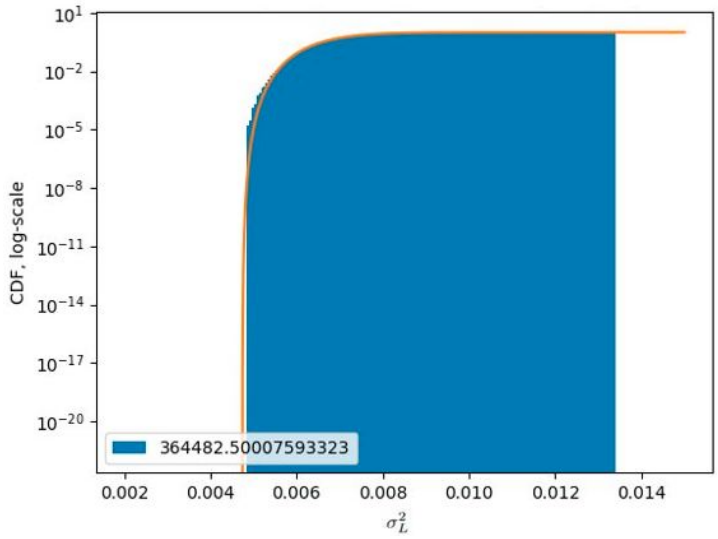

Figure 60: CDF of the σ_L^2 histogram (section 6.1.3, figure 42) which was fitted by a Gamma distribution. The fit approximates the histogram really well. Label shows the 'likelihood' value.

A.3 Gaussian model

A.3.1 Variance

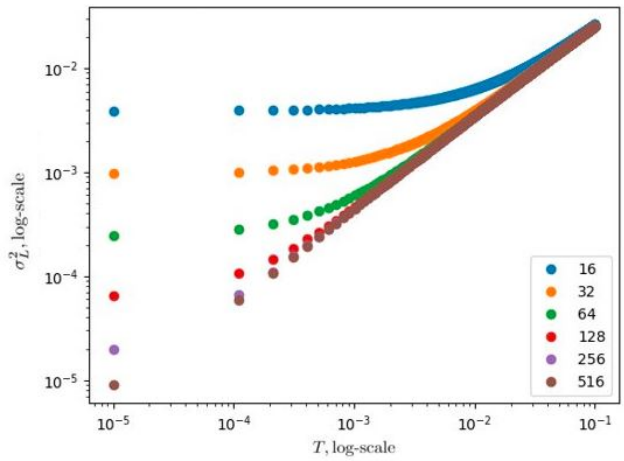

Figure 61: Analytical result for σ^2 up to $L = 516$ plotted against T. It settles for finite systems at $1/L^2$ for $T \longrightarrow 0$. For infinite systems we have $\sigma_L^2 = \sigma^2$.

A.3.2 Variances, integral approximations

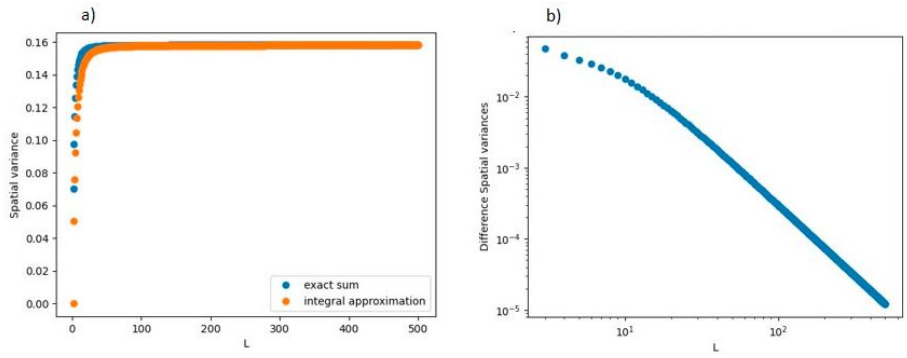

Figure 62: a) Exact sum and integral approximation for σ_L^2 (no low T expansion) plotted against L. b) The approximation converges to the sum expression for increasing $L \longrightarrow \infty$. σ_L^2 does not diverge for large L.

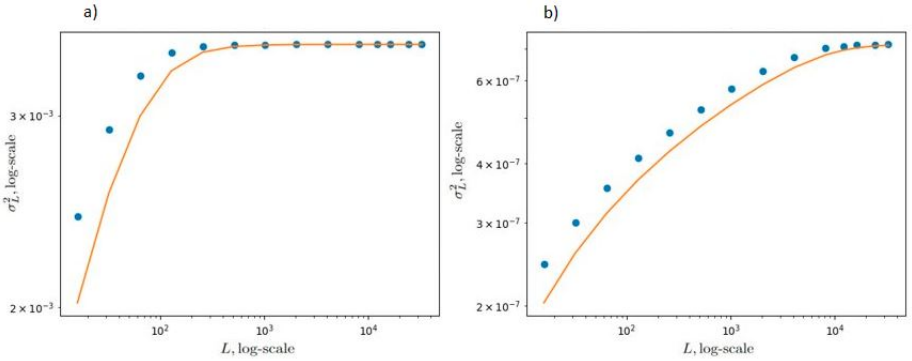

Figure 63: Analytical results for taking the limit $L \longrightarrow \infty$ without a linear temperature expansion and setting T to a small value below T_{fs}. a) For $T = 10^{-2}$ and b) $T = 10^{-6}$.

A.4 Ornstein-Zernike form

$|\vec{k}| := k$, $\vec{r} := r$, d is the spatial dimension, $G(-r) = G(r)$ (conjugate symmetry for real functions), $\kappa \propto \sqrt{T - T_c}$ for $T \geq T_c$ is related to the inverse correlation length ξ. The calculation is adapted from [60].

$$\mathcal{F}(\mathcal{F}(G(r))) = G(r) \propto \int d\vec{k} \frac{e^{i\vec{k}\vec{r}}}{k^2 + \kappa^2} = \int d\vec{k} e^{i\vec{k}\vec{r}} \int_0^\infty dt e^{-t(k+\kappa^2)}$$

$$= \int_0^\infty dt e^{-t\kappa^2} \int d\vec{k} e^{-tk^2 + i\vec{k}\vec{r}} = \int_0^\infty dt e^{-t\kappa^2} \int d\vec{k} e^{-t(\vec{k} - \frac{i}{2t}\vec{r})^2 - \frac{r^2}{4t}}$$

$$= \int_0^\infty dt \left(\frac{\pi}{t}\right)^{\frac{d}{2}} e^{-t\kappa^2 - \frac{r^2}{4t}}$$

where we completed the square in the second last equality. For $T = T_c$ the correlation length diverges and we can neglect κ, e.g. $\kappa = 0$. Also

$$G(r) \propto \int_0^\infty dt \left(\frac{\pi}{t}\right)^{\frac{d}{2}} e^{-\frac{r^2}{4t}} = \left(\frac{r^2}{4}\right)^{1-\frac{d}{2}} \pi^{\frac{d}{2}} \Gamma(\frac{d}{2} - 1) \propto \frac{1}{r^{d-2}}$$

Where Γ is the gamma function. Per definition: $G(r) \propto (r^{d-2+\eta})^{-1}$; thus $\eta = \eta_{MF} = 0$.

References

[1] Lands, W. E. 1960. Metabolism of glycerolipids. 2. The enzymatic acylation of lysolecithin. J. Biol. Chem. 235:2233–2237.

[2] Simons, K., and E. Ikonen. 1997. Functional rafts in cell membranes. Nature. 387:569–572.

[3] Honerkamp-Smith, A. R., S. L. Veatch, and S. L. Keller. 2009. An introduction to critical points for biophysicists; observations of compo- sitional heterogeneity in lipid membranes. Biochim. Biophys. Acta. 1788:53–63.

[4] Carpenter, T. S., C. A. Lopez, ., S. Gnanakaran. 2018. Capturing phase behavior of ternary lipid mixtures with a refined martini coarse-grained force field. *J. Chem. Theory Comput.* 14:6050–6062.

[5] Ingólfsson, H. I., M. N. Melo, ., S. J. Marrink. 2014. Lipid organiza- tion of the plasma membrane. J. Am. Chem. Soc. 136:14554–14559.

[6] Robert E. Scott, Plasma Membrane Vesiculation: A New Technique for Isolation of Plasma Membranes. *Science 194*,743-745 (1976).

[7] Kaiser, H.-J., D. Lingwood, ., K. Simons. 2009. Order of lipid phases in model and plasma membranes. Proc. Natl. Acad. Sci. USA. 106:16645–16650.

[8] Veatch, S. L., P. Cicuta, ., B. Baird. 2008. Critical fluctuations in plasma membrane vesicles. ACS Chem. Biol. 3:287–293.

[9] Girard, M., and T. Bereau. 2021. Finite-size transitions in complex membranes. Biophys. J. 120:2436–2443.

[10] Huang, Kerson (1987). Statistical Mechanics. *Wiley*.

[11] Dekking, Michel (2005). A Modern Introduction to Probability and Statistics. *Springer*, chapter 13.

[12] Montgomery, Douglas C.; Runger, George C. (2014). Applied Statistics and Probability for Engineers (6th ed.). *Wiley*, chapter 7.

[13] Landau, L.D.; Lifshitz, E.M. (1980). Statistical Physics. *Pergamon Press*.

[14] Lê Nguyên Hoang, Science4All - Quality popular science by Lê.

[15] A to Z of Thermodynamics - Pierre Perrot, *Oxford University Press*.

[16] Salavati, Mohammad. 2020. Multi-Scale Modeling of Mechanical and Electrochemical Properties of 1D and 2D Nanomaterials, Application in Battery Energy Storage Systems.

[17] Reichl, Linda (1980). A Modern Course in Statistical Physics. *Edward Arnold*.

[18] Gibbs, Josiah Willard (1902). Elementary Principles in Statistical Mechanics. *New York: Charles Scribner's Sons*.

[19] Jaynes, Edwin T (1996). "The Gibbs Paradox" (PDF). Retrieved November 8, 2005.

[20] Robert A. Alberty - Legendre transforms in chemical thermodynamics. *Pure Appl. Chem.*, Vol. 69, No. 11, pp. 2221-2230, 1997.

[21] Einstein, Albert (May 1905). "Über die von der molekularkinetischen Theorie der Wärme geforderte Bewegung von in ruhenden Flüssigkeiten suspendierten Teilchen". Annalen der Physik. 322 (8): 549–560.

[22] C. Domb, M. S. Green, J. L. Lebowitz (Hrsg.): Phase Transitions and Critical Phenomena. Band 1–20 (1972–2001). *Academic Press*.

[23] Christopher AuYeung, CK-12 Foundation, *FlexBooks 2.0*.

[24] Jaeger, Gregg (1 May 1998). "The Ehrenfest Classification of Phase Transitions: Introduction and Evolution". *Archive for History of Exact Sciences*. 53 (1): 51–81.

[25] Muhammad Wasif, Sabieh Anwar (2010). Studying Phase Transitions with a Strain Gage. *ResearchGate*.

[26] Meike Kloster - Gittergase. 2006.

[27] Wikipedia, edited by 'BlyumJ' (username) - Entropy of mixing. May 2023

[28] V. L. Ginzburg (1961). "Some remarks on phase transitions of the 2nd kind and the microscopic theory of ferroelectric materials". Soviet Physics - Solid State. 2: 1824.

[29] Pitzer, K. S. Thermodynamics, 3rd ed., chapter 3; McGraw-Hill: New York, 1995.

[30] Dissemination of IT for the Promotion of Materials Science (DoITPoMS) University of Cambridge - Free energy curves.

[31] K. Binder, P. Fratzl "Spinodal Decomposition" in Phase Transformations in Materials (G. Kostorz, ed.) Wiley-VCH, Weinheim (2001), pp. 409-480.

[32] J. M. Smith, H. C. Van Ness, M. M. Abbott, M. T. Swihart (2018) - Introduction to Chemical Engineering Thermodynamics. *McGraw-Hill Education*

[33] Wikipedia, by 'Maksim' (username) - Renormalization group. May 2023

[34] Kadanoff, Leo P. (1966). Scaling laws for Ising models near T_c. *Physics Physique Fizika.*.

[35] Daniel Arovas (2018) - Thermodynamics and Statistical Mechanics, chapter 9.3.

[36] A. Sandvik, ICTP School in Computational Condensed Matter Physics, Lecture 3 (2015).

[37] Berezinskii, V. L. (1971), "Destruction of long-range order in one-dimensional and two-dimensional systems having a continuous symmetry group I. Classical systems", Sov. Phys. JETP, 32 (3): 493–500.

[38] Sacha Friedli and Yvan Velenik (2017). Statistical Mechanics of Lattice Systems: A Concrete Mathematical Introduction. *Cambridge: Cambridge University Press*.

[39] Polyakov, A.M. (1975). "Interaction of goldstone particles in two dimensions. Applications to ferromagnets and massive Yang-Mills fields". Phys. Lett. B 59 (1): 79–81.

[40] P. Schmoll, A. Kshetrimayum, J. Eisert, R. Orus, M. Rizzi (2021). The classical two-dimensional Heisenberg model revisited: An SU(2)-symmetric tensor network study. SciPost Phys. 11, 098.

[41] Connie Rye, Robert Wise, Vladimir Jurukovski, Jean DeSaix, Jung Choi, Yael Avissar (2016). Biology, chapter 5.1. *OpenStax*.

[42] Sadava D, Hillis DM, Heller HC, Berenbaum MR (2011). Life: The Science of Biology 9th Edition. San Francisco: Freeman. pp. 105–114.

[43] Katalin Nagy and Ioana-Daria Tiuca(2017). Importance of Fatty Acids in Physiopathology of Human Body. Chapter 1 of book *Fatty Acids* by Angel Catala. *InTechOpen*

[44] Bretscher, Mark S. (1 March 1972). "Asymmetrical Lipid Bilayer Structure for Biological Membranes". *Nature New Biology*. 236 (61): 11–12.

[45] Baumgart, T., A. T. Hammond, ., W. W. Webb. 2007. Large-scale fluid/fluid phase separation of proteins and lipids in giant plasma mem- brane vesicles. Proc. Natl. Acad. Sci. USA. 104:3165–3170.

[46] Bendix, P.M.; Simonsen, A.C.; Florentsen, C.D.; Häger, S.C.; Mularski, A.; Zanjani, A.A.H.; Moreno-Pescador, G.; Klenow, M.B.; Sønder, S.L.; Danielsen, H.M.; Arastoo, M.R.; Heitmann, A.S.; Pandey, M.P.; Lund, F.W.; Dias, C.; Khandelia, H.; Nylandsted, J. Interdisciplinary Synergy to Reveal Mechanisms of Annexin-Mediated Plasma Membrane Shaping and Repair. Cells 2020, 9, 1029.

[47] Veatch, S. L., P. Cicuta, ., B. Baird. 2008. Critical fluctuations in plasma membrane vesicles. *ACS Chem. Biol.* 3:287–293.

[48] Benjamin B. Machta, Stefanos Papanikolaou, James P. Sethna, and Sarah L. Veatch (2011). Minimal Model of Plasma Membrane Heterogeneity Requires Coupling Cortical Actin to Criticality. *Biophys J.*. 100(7):1668-77.

[49] A. G. Clamp, S. Ladha, D. C. Clark, R. F. Grimble, E. K. Lund (1997). The influence of dietary lipids on the composition and membrane fluidity of rat hepatocyte plasma membrane. *Wiley*.

[50] Hastings, W.K. (1970). "Monte Carlo Sampling Methods Using Markov Chains and Their Applications". *Biometrika*. 57 (1): 97–109.

[51] Daan Frenkel, Berend Smit (2002). Understanding Molecular Simulation. *Academic Press*.

[52] Giovanni Settanni. Moderne Rechenmethoden der Physik kondensierter/weicher Materie. Lecture series SoSe 2021.

[53] LAMMPS Course for Intermediate Users - Replica exchange (2019).

[54] Fernando M. S. Silva Fernandes and Rui P. S. Fartaria (2015). Gibbs ensemble Monte Carlo. *Computational physics*.

[55] Bernhard A. Wolf. Interaction parameters. Johannes-Gutenberg Universitaet Mainz.

[56] Norbert Wiener (1964). Time Series. *M.I.T. Press*, Cambridge, Massachusetts. p. 42.

[57] TALOS documentation (2023). Max-Planck Computing and Data Facility.

[58] Mattis, D.C. (1984). "Transfer matrix in plane-rotator model". *Physics Letters* A. 104 A (6–7): 357–360.

[59] Philipp Schmoll, Augustine Kshetrimayum, Jens Eisert, Román Orús, Matteo Rizzi (2021). The classical two-dimensional Heisenberg model revisited: An $S(U)$-symmetric tensor network study. SciPost Phys. 11, 098.

[60] Ornstein, L.S.; Zernike, F. (1914). "Accidental deviations of density and opalescence at the critical point of a single substance" (PDF). *Proceedings of the Royal Netherlands Academy of Arts and Sciences*. 17: 793–806.

[61] Corradi, V., E. Mendez-Villuendas, ., D. P. Tieleman. 2018. Lipidprotein interactions are unique fingerprints for membrane proteins. *ACS Cent. Sci.* 4:709–717.

[62] Schmid, F. 2017. Physical mechanisms of micro- and nanodomain formation in multicomponent lipid membranes. Biochim. Biophys. Acta Biomembr. 1859:509–528.

[63] Luo J, Yang H, Song BL. Mechanisms and regulation of cholesterol homeostasis. Nat Rev Mol Cell Biol. 2020 Apr;21(4):225-245.

[64] Nguyen, P.H.; Boninsegni, M. (2021). "Superfluid Transition and Specific Heat of the 2D x-y Model: Monte Carlo Simulation". Applied Sciences. 11 (11): 493.

B Acknowledgements

I would like to thank my supervisor Martin Girard for being a reliable mentor and helping me with fast and helpful feedback.

Additionally I want to thank Burkhard Dünweg for insightful discussions and teachings, as well as Friederike Schmid for insightful feedback regarding the project. I also want to thank all members of the Theory group of Kurt Kremer at the Max-Planck institute for polymer science for integrating me into the group, for discussions and their support.

Finally I want to thank my friends and family for being in my life.